Garnierites and garnierites: Textures, mineralogy and geochemistry of garnierites in the Falcondo Ni-laterite deposit, Dominican Republic

Cristina Villanova-de-Benavent, Joaquin A. Proenza, Salvador Gali, Antonio Garcia-Casco, Esperanca Tauler, John F. Lewis, Francisco Longo

PII: S0169-1368(13)00233-3
DOI: doi: 10.1016/j.oregeorev.2013.10.008
Reference: OREGEO 1124

To appear in: *Ore Geology Reviews*

Received date: 24 May 2013
Revised date: 22 October 2013
Accepted date: 23 October 2013

Please cite this article as: Villanova-de-Benavent, Cristina, Proenza, Joaquin A., Gali, Salvador, Garcia-Casco, Antonio, Tauler, Esperanca, Lewis, John F., Longo, Francisco, Garnierites and garnierites: Textures, mineralogy and geochemistry of garnierites in the Falcondo Ni-laterite deposit, Dominican Republic, *Ore Geology Reviews* (2013), doi: 10.1016/j.oregeorev.2013.10.008

- TITLE: Garnierites and garnierites: textures, mineralogy and geochemistry of garnierites in the Falcondo Ni-laterite deposit, Dominican Republic.
- TITLE PAGE: Garnierites in Falcondo Ni-laterite: textures, mineralogy and geochemistry.
- AUTHORS AND AFILIATIONS:

Cristina Villanova-de-Benavent (corresponding author)
Departament de Cristal·lografia, Mineralogia i Dipòsits Minerals
Facultat de Geologia
Universitat de Barcelona
Martí i Franquès s/n
08028 Barcelona
Catalonia, Spain
e-mail: cvillanovadb@ub.edu
Phone: 00 34 93 402 13 41
Fax: 00 34 93 402 13 40

Joaquín A. Proenza
Departament de Cristal·lografia, Mineralogia i Dipòsits Minerals
Facultat de Geologia
Universitat de Barcelona
Martí i Franquès s/n
08028 Barcelona
Catalonia, Spain

Salvador Galí
Departament de Cristal·lografia, Mineralogia i Dipòsits Minerals
Facultat de Geologia
Universitat de Barcelona
Martí i Franquès s/n
08028 Barcelona
Catalonia, Spain

Antonio García-Casco
Department of Mineralogy and Petrology (Universidad de Granada) and Andalusian Institute of Earth Sciences (IACT, UGR-CSIC)
Campus Fuentenueva s/n
18071 Granada
Spain

Esperança Tauler
Departament de Cristal·lografia, Mineralogia i Dipòsits Minerals
Facultat de Geologia
Universitat de Barcelona

Martí i Franquès s/n
08028 Barcelona
Catalonia, Spain

John F. Lewis
Department of Earth and Environmental Sciences
The George Washington University
20052 Washington D.C.
USA

Francisco Longo

Falcondo Glencore
Box 1343 Santo Domingo
Dominican Republic

- ABSTRACT:

Garnierites (Ni-Mg-bearing phyllosilicates) are significant ore minerals in Ni-laterites of the hydrous silicate-type. In the Falcondo Ni-laterite deposit (Dominican Republic), garnierites are found within the saprolite horizon mainly as fracture-fillings and thin coatings on joints. Field observations indicate an important role of active brittle tectonics during garnierite precipitation. Different greenish colours and textures can be distinguished, which correspond to different mineral phases, defined according to X-ray diffraction (XRD) and electron microprobe (EMP) analyses: a) talc-like (10 Å-type), b) serpentine-like (7 Å-type), c) a mixture of talc- and serpentine-like, and d) sepiolite-like types. Compositional data indicate continuous Mg-Ni solid solution along the joins lizardite-népouite (serpentine-like), kerolite-pimelite (talc-like) and sepiolite-falcondoite (sepiolite-like). In general, talc-like garnierite is dominant in Falcondo Ni-laterite and displays higher Ni contents than serpentine-like garnierites. EMP analyses showing deviations from the stoichiometric Mg-Ni solid solutions of serpentine and talc are best explained by talc- and serpentine-like mixing at the nanoscale. A detailed textural study by means of quantified X-ray element imaging provides a wealth of new information about the relationships between textural position, sequence of crystallization and mineral composition of the studied garnierite samples. These results indicate several stages of growth with variable Ni content, pointing to recurrent changes in the physical-chemical conditions during garnierite precipitation. In addition, our detailed mineralogical study of the Falcondo garnierites revealed that the different types identified have characteristic H_2O content and SiO_2/MgO ratios, which play important roles during the pyrometallurgy process.

- KEYWORDS:

garnierite; Ni-laterite; Dominican Republic; lizardite-népouite; kerolite-pimelite; sepiolitefalcondoite

1. Introduction

Although Ni (±Co) laterite deposits account only for about 40% of the current world's annual Ni production, they host over 60% of the world land-based Ni resources (Gleeson *et al*., 2003; Kuck, 2013), and the amount of Ni being extracted from laterite ores is increasing steadily (Mudd, 2010). About 10% of the world's Ni resources are found in the Caribbean region, mostly in the northern part, and include the Moa Bay and Punta Gorda deposits in eastern Cuba and the Falcondo deposit in central Dominican Republic (Dalvi *et al*., 2004; Lewis *et al*., 2006; Nelson *et al*., 2011). Other Ni-laterite deposits in the region include the Gloria deposit in Guatemala (Golightly, 2010) and the Meseta de San Felipe deposit in Camagüey in Central Cuba (Gallardo *et al*., 2010a). On the other hand, the major Ni laterite resources in the southern Caribbean include the Cerro Matoso in Colombia (Gleeson *et al*., 2004) and Loma de Hierro in Venezuela (Soler et al., 2008), both presently exploited.

Ni (±Co) laterite deposits are regoliths formed by the chemical weathering of ultramafic rocks, mainly in tropical and subtropical latitudes (e.g. Golightly, 1981; Elias, 2002; Freyssinet *et al*., 2005). Under the high temperature and intense rainfall, typical of these environments, the most soluble elements (especially Mg and Si) are leached from primary rock-forming ferromagnesian minerals, and the least mobile elements (especially Fe, Al) accumulate in successive horizons of the lateritic profile (e.g. Freyssinet *et al*., 2005; Golightly, 2010).

Although there is no widely accepted terminology and classification, Ni (±Co) laterites are commonly classified into three categories, according to the main Ni ore assemblage (Brand *et al*., 1998). These include: i) Oxide laterite deposits in which the ore assemblage is principally Fe oxyhydroxides; ii) Clay silicate deposits dominated by Ni-rich smectites; and iii) Hydrous Mg silicate deposits in which the ore is mainly Mg-Ni phyllosilicates (including garnierites). The hydrous Mg silicate deposits generally have the highest Ni grade (1.8–2.5 wt.% Ni) and are characterised by a thick serpentine-dominated saprolite horizon covered by a relatively thin Fe-oxyhydroxide-dominated limonite horizon (laterite *sensu stricto* horizon). These deposits are formed under conditions of a low water table and continuous tectonic uplift (Freyssinet *et al*., 2005; Butt and Cluzel, 2013).

In terms of production and reserves, the Falcondo deposit is the largest hydrous Mg silicate-type Ni-laterite deposit of the Greater Antilles, with estimated Ni reserves of about 79.2 million dry tonnes at a grade of 1.3 wt.% Ni (Falcondo Annual Report, 2010; http://www.falcondo.com.do/ES/Publicaciones/brochures/Memoria_FALCONDO_2010.pdf). As other hydrous Mg silicate-type deposits worldwide, Ni-bearing serpentines and particularly garnierites are concentrated in the lowermost part of the saprolite horizon, toward the base of the profile (Freyssinet *et al*., 2005).

The term garnierite is generally used to refer to the group of green, fine-grained poorly crystallized Ni-bearing magnesium phyllosilicates, which include serpentine, talc, sepiolite, smectite and chlorite; often occurring as mixtures (e.g. Faust, 1966; Brindley and Hang, 1973; Springer, 1974; Brindley, 1978). Although garnierite is not recognized as a mineral species by the International Mineralogical Association (IMA), it is a convenient field term used by mine geologists for all green Ni-silicates when more specific characterization is not possible (Brindley, 1978).

The classification and nomenclature of garnierite-forming minerals remain controversial because of their fine-grained nature, poor crystallinity and frequent occurrence as intimate mixtures of different mineral species. After various studies (Brindley and Hang, 1973; Brindley and Maksimović, 1974; Brindley, 1978; 1980), Brindley and co-authors distinguished two groups of garnierites: i) 1:1 and ii) 2:1 layer minerals. The first group includes the Mg-Ni series of the serpentine group minerals: lizardite-népouite, chrysotile-pecoraite and berthierine-brindleyite. The second group comprises the following Mg-Ni series: talc-willemseite, kerolite-pimelite, clinochlore-nimite, and sepiolite-falcondoite.

The most common garnierite minerals found in nature are lizardite-népouite and kerolite-pimelite (Brindley, 1978). For these minerals, the terminology “serpentine-like” (or 7 Å-type) and “talc-like” (or 10 Å-type) garnierites, respectively, has been widely used (Brindley and Hang, 1973, Brindley and Maksimović, 1974; Wells *et al*., 2009; Galí *et al*., 2012). It is important to note here that the term “talc-like” does not refer to the normal composition and/or structure of talc (Brindley and Hang, 1973). Actually, the characterisation of talc-like garnierites is controversial and both the Mg and Ni talc-like end members kerolite and pimelite, respectively, are discredited mineral species by the IMA. Despite being historically described as hydrated talc-like minerals, kerolite

and pimelite were classified into the smectite group by Faust (1966). In contrast, other authors proved a structure with talc affinity, since kerolite and pimelite do not exhibit intracrystalline swelling (e.g. Slansky, 1955; Kato, 1961; Maksimović, 1973; Brindley and Hang, 1973). In addition, an intermediate phase between talc-like and serpentine-like end members, karpinskite $(Mg,Ni)_2Si_2O_5(OH)_2$, was described by Rukavishnikova (1956), however it is not accepted as a mineral species by the IMA.

Several mineralogical studies using different techniques have been published on garnierites since their discovery in 1864, most of them during the late 1960s to early 1980s. The majority of the publications since the 1960's focussed on the composition of garnierites from New Caledonia (Caillère, 1965; Troly *et al.*, 1979; Pelletier, 1983; 1996), Indonesia (Golightly, 1979) and Australia (Elias *et al.*, 1981). It is only in the past few years that detailed additional information, including mode of occurrence in the field, petrography and relations between garnierites and their host rocks, is provided (Cluzel and Vigier, 2008; Wells *et al.*, 2009).

In the case of Falcondo Ni-laterite deposits, as a result of the Al-poor nature of the ultramafic protolith, previous results have shown that garnierites consist mainly of the combination of three solid solutions: serpentine-like $[(Mg,Ni)_3Si_2O_5(OH)_4]$, talc-like $[(Mg,Ni)_3Si_4O_{10}(OH)_2\cdot(H_2O)]$ and sepiolite-falcondoite $[(Mg,Ni)_4Si_6O_{15}(OH)_2\cdot 6(H_2O)]$ (Proenza et al., 2008; Tauler *et al*., 2009; Galí *et al*., 2012). However, except for the sepiolite-falcondoite series (Springer, 1976; Tauler et al., 2009), little work has been done on the mode of occurrence, textures and composition of these Ni-phyllosilicates.

In this paper we summarize the information on the garnierites from the Falcondo Ni-laterite deposit up to the present, and provide detailed descriptions of their occurrence in the field and textural relationships, as well as new results on mineralogy and mineral chemistry. Our study focuses on serpentine- and talc-like garnierite, presents data from the saprolite host and also includes new information on the sepiolite-falcondoite garnierite. The aim of this work is to gain further insight into the origin of garnierites in the Falcondo deposit.

2. The Ni-laterite deposit of Falcondo

2.1. Geological setting

The main nickel laterite deposits in the central Dominican Republic occur over the serpentinised Loma Caribe peridotite belt (Fig. 1), which is about 4–5 km wide and extends NW for 95 km from La Vega to Loma Sierra Prieta, north of Santo Domingo; its south-eastern part is exposed as thin fault slices (Lewis and Jiménez, 1991, Lewis *et al.*, 2006). The peridotite is interpreted, from airborne magnetics and drilling, to extend south-eastward below the surface to the coast (Lewis et al., 2006). The Loma Caribe belt is bounded by reverse faults dipping eastward at 75–80º (Mann et al., 1984). The major faults within the body are shear zones that strike parallel to the northwest trend of the belt and the foliation of the serpentinised peridotite. These faults and other basic structures in the central area of the Loma Caribe peridotite massif have been mapped (Haldemann et al., 1979; Fig. 1), although they have not been systematically studied.

The Loma Caribe peridotite forms the core of a Mesozoic age Median Belt (Bowin, 1966; Lewis and Draper, 1990), which includes two major metavolcanic units: 1) the Maimón Formation (Fm.) to the northeast of the peridotite belt represents a primitive island arc tholeiitic unit of Lower Cretaceous age, and 2) the Duarte Complex to the southwest of the peridotite belt formed by mantle plume–related oceanic plateau basalts of Upper Jurassic-Lower Cretaceous age (Lewis *et al*., 2002). The Maimón Fm. is unconformably overlain by the Siete Cabezas Fm. (volcanic arc basalts with minor tuffs and wackes of Cenomanian age), and the Duarte Fm. is unconformably overlain by the Peralvillo Fm. (volcanic arc andesites, diorites, basalts, tuffs, breccias and conglomerates of Late Cretaceous age; Haldemann *et al*., 1979; Lewis *et al*., 2002; Proenza *et al*., 2007). The peridotite belt also hosts some dolerite dykes. In addition, diorite bodies outcrop along the faulted margins of the peridotite belt, and some gabbroic intrusives occur in the Peralvillo Fm. (Fig. 1; Lithgow, 1993; Escuder-Viruete et al., 2006).

Based on the mineralogy and textural features of the ultramafic rocks, the Loma Caribe peridotite was interpreted by Lewis and Jiménez (1991) as a (serpentinised) harzburgitic oceanic mantle forming part of a dismembered ophiolite complex. The ultramafic body includes podiform chromitite pods within dunites and suggests that most of the peridotite is part of the transition zone of the mantle section of harzburgite-type alpine peridotite complexes.

The Loma Caribe ultramafic rocks originally formed in the upper mantle below an evolving suprasubduction oceanic lithosphere (Lewis *et al*., 2006). We infer that the peridotites would have likely been partially serpentinised by the hydrothermal reaction of oceanic water with the mantle rock as they moved upwards through the forearc/arc lithosphere prior to their final emplacement in their current crustal tectonic position. The tectonic emplacement occurred as early as the late Albian, as a result of the collision of an oceanic plateau (the Duarte plateau terrane) with the primitive Caribbean island–arc (Maimón-Amina terrane) at Aptian time (Lewis *et al*., 2002). This event resulted in the northward emplacement (obduction) of the peridotite over the Maimón Formation. In the middle to late Eocene, Hispaniola underwent southwest contraction (Mann *et al*., 1991). Many of the mid-Cretaceous thrust structures were reactivated at this time, resulting in thrusting of the peridotite in a northeast direction over the Peralvillo Fm. (Draper *et al*., 1996). Uplifting of the northwestern margin of the Cordillera Central occurs along three reverse or thrust mapped faults (Bonao, Hatillo and Hispaniola Fault Zones). The northwesterly striking segment of the Oligocene age strike-slip Hispaniola Fault Zone comprises the Loma Caribe ultramafic body (Mann et al., 1984). Further exhumation of the peridotite in the Oligocene is well-documented in the La Vega area (Lewis and Jiménez, 1991).

Both "fresh" and serpentinised peridotites have been exposed to weathering and erosion since the early Miocene. These processes were followed by uplift, block faulting and subsequent cycles of laterisation (Haldemann *et al.*, 1979). The Miocene land surface was broken into blocks by vertical movements related to transpressional deformation along major faults. At least four physiographic cycles have been recognised corresponding to different surface levels (Lewis *et al*., 2006). Geomorphological observations indicate that block-faulting postdates the first of the laterisation cycles (Haldemann *et al*., 1979).

Under supergene conditions, the serpentinised peridotites of Loma Caribe evolved in a similar way to that of the ophiolite-related, hydrous Mg silicate deposits found (and exploited) in the arcs of the West Pacific, e.g. in the Philippines, Indonesia and New Caledonia (Golightly, 2010).

2.2. The Ni-laterite profile

As other hydrous silicate-type Ni-laterite deposits, the weathering profile in Falcondo is divided into three main horizons: the unweathered protolith at the bottom, a thick saprolite horizon and a limonite horizon at the top (Fig. 2). However, the mine geologists have subdivided profile into six zones (A to F) on the basis of nickel and iron contents, texture, and proportion of rocky fragments. These zones are, from the base to the top: unweathered ultramafic (F), serpentinised peridotite (E), hard serpentine (D), soft serpentine (C), lower limonite (B) and upper limonite (A), which may be covered by a hematitic cap (Fig. 2; Haldemann *et al*., 1979; Lithgow, 1993; Lewis *et al*., 2006). The zones E, D and C represent the saprolite horizon, whereas the zones B and A correspond to the limonite horizon. The thickness of the laterite profile varies from 1 to 60 meters (Haldemann *et al*., 1979). Likewise, the thickness of the different zones in the profile varies vertically and laterally in all exposures in the Falcondo deposit (Fig.6 in Lewis *et al.*, 2006).

The unweathered ultramafic protoliths are clinopyroxene-rich harzburgite, lherzolite, fine-grained black dunite and sheared dark green serpentinite. In general, the major constituent of the host ultramafic rocks is olivine (Fo_{89-92}, 0.35–0.55 wt.% NiO) followed by orthopyroxene (En_{89-92}, NiO < 0.1 wt.%) and minor clinopyroxene (#Mg = 86–95) (Haldemann *et al.*, 1979; Lithgow, 1993; Lewis *et al.*, 2006; Marchesi *et al.*, 2012).

The main mining areas being exploited by Falcondo Glencore include, from north to south: Loma Ortega, Caribe, Fraser, Taína, Larga, Guardarraya and Peguera (Fig. 1). The flat summit levels of Guardarraya, Peguera and Taína occur at an elevation of 610 ± 40 m. They are remnants of the Miocene land surface which had undergone laterisation followed by uplifting, block-faulting and subsequent cycles of laterisation (Haldemann *et al.*, 1979).

2.3. Mode of occurrence of garnierites in the Falcondo Ni-laterite deposit

Garnierite mineralisation exposed in the mining pit are concentrated in discrete zones from tens to one hundred metres long and up to five metres thick (Fig. 3a, b). They are found mainly within the lowermost part of the saprolite horizon (Fig. 3c) as well as in unweathered serpentinised peridotite at the base of the profile (Fig. 3d) and in the soft serpentine zone in the upper saprolite horizon (Fig. 3e).

The garnierites occur mainly as mm-cm veins in fractures (Fig. 3c-h), as well as thin coatings on joints and fault planes which are oriented in random directions (Fig. 3i-k). The coatings on fault plane surfaces commonly contain slickensides (Fig. 3l). Garnierites are also found in two different kinds of breccias: i) weathered serpentinised ultramafic rock (saprolite) fragments cemented by garnierite, and ii) silicified Ni-sepiolite fragments cemented by a later generation of garnierite. In addition, another type of breccia is found in the laterite profile, not containing garnierite, and consisting of saprolite clasts cemented by Ni-free sepiolite and silica/quartz (Fig. 3m, n).

The garnierites occur in various shades of green. Apart from the sepiolite-falcondoite species, with typical white to pale green colour and remarkable schistosity, four types of garnierite have been distinguished according to their colour and will be hereafter named type I to IV: Type I is yellowish pale green, type II is apple green, type III is dark green, and type IV is bluish green. Type IV is the dominant phase and the other phases are less common but quite distinctive. Type I occurs as millimetre-thick infillings in fractures (Fig. 3c). Types II and III form millimetre to centimetre-scale fracture infillings and coatings (Fig. 3c, g, i). Finally type IV occurs as thin coatings and fillings in fractures (Fig. 3g), and coexists with other garnierite types, typically superimposed to the yellowish green and apple green types. In addition, all the above four types of garnierites also occur as cementing material in breccia with saprolite clasts. Finally, the sepiolite-falcondoite (classified here as type V) commonly forms centimetre-thick vein fillings (Fig. 3h).

3. Materials and methods

3.1. Sampling

A total of forty samples were collected from the saprolite horizon of different *lomas* in the Falcondo Ni-laterite deposit. The samples were analysed by X-ray powder diffraction (XRD), optical and scanning electron microscopy (SEM-EDS) and electron microprobe (EMP) for their mineralogical and chemical characterization. From the forty samples, twelve were selected as the most representative of the different types of garnierites described above (Table 1, Fig. 4). All analyses were performed in the Centres Científics i Tecnològics of the Universitat de Barcelona, Spain.

3.2. Analytical and computation techniques

3.2.1. X-ray powder diffraction (XRD)

In order to obtain the most pure phase specimens for XRD, different greenish-coloured garnierite types were carefully separated hand-picking and ground in an agate mortar. Powder specimens were set in standard cylindrical sample holders (16 mm of diameter and 2.5 mm thick) by manual pressing using a glass plate to get a flat surface. Diffractograms were obtained in a PANalytical X'Pert PRO MPD Alpha1 powder diffractometer in Bragg-Brentano θ/2θ geometry of 240 mm of radius, nickel filtered Cu Kα radiation (λ = 1.5418 Å), 45 kV and 40 mA.

During the analysis, the sample was spun at 2 revolutions per second. A variable divergence slit kept the area illuminated constant (10 mm) and a mask used to limit the length of the beam (12 mm). Axial divergence Soller slits of 0.04 radians were used. Samples were scanned from 3 to 80º 2θ with step size of 0.017º and measuring time of 50 seconds per step, using a X'Celerator detector (active length = 2.122º).

3.2.2. Electron Microprobe (EMP)

Polished thin sections previously examined in an Environmental Scanning Electron Microscope (ESEM) Quanta 200 FEI, XTE 325/D8395 were analysed with a Cameca Electron Microprobe Analyser SX-50, equipped with four wavelength dispersive spectrometers and an energy dispersive spectrometer. The operation conditions were 20 kV, 15 nA, 2 µm beam diameter and counting time of 20 s per element. The calibration standards used were: hematite (Fe, LIF, Kα), rutile (Ti, PET, Kα), periclase (Mg, TAP, Kα), rodonite (Mn, LIF, Kα), Al_2O_3 (Al, TAP, Kα), Cr_2O_3 (Cr, PET, Kα), diopside (Si, TAP, Kα), NiO (Ni, LIF, Kα) and wollastonite (Ca, PET, Kα).

Talc-like, serpentine-like and sepiolite analyses were normalized to 11, 7 and 32 oxygens, respectively. The atomic concentration of elements per formula unit is abbreviated apfu. Mineral and end member abbreviations are after Whitney and Evans (2010), except for falcondoite (Fal), kerolite (Ker), pimelite (Pim) and népouite (Nep) following Tauler *et al.* (2009) and Galí *et al.* (2012), and karpinskite (Krp).

Back-scattered electron (BSE) and elemental X-ray (XR) maps of Si, Fe, Mg, Ni and Al were obtained by averages of WDS scanning of the samples using the same machine operated at 20 keV and 200 nA or 100 nA (noted in the figures), a focused beam of 5 µm, step (pixel) size of 3 µm, and counting time of 20–30 ms/pixel. High beam current combined with short counting time (milliseconds) avoids beam damage to silicate

minerals (García-Casco, 2007). The element maps were processed with *DWImager* software in order to show particular textures and mineral composition features (Torres-Roldán and García-Casco, unpublished). The images represent quantified maps obtained with the same software following the procedure of Bence and Albee (1968) for matrix correction and using an internal mineral standard of the mineral of interest analyzed with the microprobe in the scanned areas (as indicated in the figures) and the α-factor table of Kato (2005; see also http://www.nendai.nagoya-u.ac.jp/gsd/a-factor/). These quantified images show pixel-sized analyses of minerals of interest expressed in atoms per formula unit and atomic ratios (color code) and indicated in the figure captions. In all quantitative map images, mineral phases not considered for illustration are masked out, and the resulting images are overlain onto a reference grey-scale BSE image having the same spatial resolution (pixels) and containing the basic textural information of the scanned areas.

The quantified pixels of the X-ray distribution images, appropriately filtered for minerals and/or voids and polish defects, were represented in ternary diagrams. These diagrams were calculated using *DWImager* software and are expressed as absolute frequency (colour code). Ternary diagrams with the point analyses of the same scanned area were prepared using *CSpace* software (Torres-Roldán *et al.*, 2000), and overlain onto the ternary plots obtained with *DWImager*.

4. Mineralogy and textures of the Falcondo garnierites and related rocks

The hand specimen descriptions of the twelve representative samples are summarised in Table 1 and a selection of representative photos is shown in Figure 4. Eight samples of garnierite from the saprolite horizon contain characteristic XRD patterns of talc- and serpentine-like garnierites and display the four greenish colour types reported in section 2.3 (Fig. 5). Different types of garnierite may coexist in the same sample. The other four samples were identified as Ni-sepiolite and falcondoite, respectively.

4.1. Saprolite Ni-serpentine

Saprolite, which represents the weakly weathered protolith, is the most common host for garnierites. In the studied samples, saprolite is reddish to dark brown and is crosscut by a close fine mesh of black veinlets (Fig. 4a, b) and consists mainly of serpentine and Fe oxides and oxyhydroxides. Close to the fractures and to the edges of saprolite

fragments, where the serpentinite is further altered (Fig. 4a, b), the serpentine is greenish grey to black in colour. Under the optical microscope, serpentine forms yellow veins wrapping reddish brown cores of serpentine and Fe oxides and oxyhydroxides, preserving the previous mesh textures of the serpentinised olivine. Serpentine near fractures and edges of fragments is pale yellow and show diffuse cores under the optical microscope. The groundmass of serpentine contains scattered tiny anhedral relict chromite grains, altered to ferrian chromite (Fig. 6a, b). Relict crystals of olivine and pyroxene are extremely rare. Intergrowths of a Ni-bearing talc-like phase are common near cracks, and are interpreted as replacements of serpentine (Fig. 6b, lower left).

4.2. Type I garnierite

Type I (yellowish pale green) garnierite occurs as millimetre to centimetre-thick veins in the saprolite (Fig. 4a). These veins are often crosscut or superimposed by millimetric veinlets of type IV (bluish green) garnierite and white quartz. Type I garnierite is characterized by a maximum diffraction peak between 7.26 and 7.30 Å, which coincides with the characteristic basal spacing range of the serpentine group minerals (Fig. 5a). Under the optical microscope this garnierite type consists of a yellowish brown heterogeneous material, intergrown with Fe oxyhydroxides (Fig. 6a, b). In addition, a nickeliferous talc-like phase may be present as seen in the backscattered electron image in the lower left corner of the Figure 6b.

4.3. Type II garnierite

Type II (apple green) garnierite occurs as coatings on angular saprolite fragments (Fig. 4b). The garnierite is in turn superposed by type IV garnierites and millimetre-thick veinlets of white quartz. The Type II garnierite is characterized by a very intense and sharp diffraction peak at 7.27–7.31 Å, and a lower broad peak at 9.95–10.14 Å, corresponding to the basal spacings of serpentine and talc, respectively (Fig. 5b). This suggests that the sample is a serpentine-like phase with talc-like impurities.

Under the optical microscope, this garnierite consists of colourless to yellowish, slightly anisotropic serpentine aggregates up to 0.5 mm in length, frequently enveloped by a very fine grained brownish grey fibrous matrix of a Ni-talc-like phase (Fig. 6c, d). Pores in the garnierite are systematically filled by euhedral elongated quartz crystals.

4.4. Type III garnierite

Type III (dark green) garnierite shows a characteristic dull to greasy luster, and consists of friable aggregates up to 15 cm in length (Fig. 4c).They also occur as matrix in breccias with: a) millimetre to centimetre-sized fragments, composed of fine-grained, whitish green mixture of Ni-sepiolite and quartz (Fig. 4d), and b) brownish orange, centimetre-scale, angular saprolite clasts (Fig. 4e). This dark green garnierite is characterised by a diffraction peak at 7.30–7.38 Å and a slightly broader peak at 9.86–10.46 Å, both having similar intensities (Fig. 5c) suggesting a mixture of serpentine-like and talc-like phases.

Under the optical microscope, type III garnierite occurs as greenish to intense green homogeneous coatings, frequently presenting botryoidal features, intergrown with quartz crystals (Fig. 6e). The euhedral terminations of the quartz crystals, in addition to the presence of several pores in the matrix, suggest that quartz and garnierites have grown in voids.

4.5. Type IV garnierite

Type IV (bluish green) garnierite occurs as millimetre to centimetre-sized coatings superimposed over other garnierite types and saprolite fragments (Fig. 4a, b). It also occurs as cement in breccias with centimetre to millimetre-size, rounded, brownish orange saprolite clasts. The saprolite clasts may contain narrow greenish white quartz veinlets (Fig. 4f), and up to 2 cm long rounded, non-spherical granules embedded in a greenish white, microcrystalline quartz matrix coexisting with millimetric angular, dark brown and/or orange saprolite fragments (Fig. 4g). Type IV garnierite shows a broad diffraction peak at 9.58–10.02 Å suggesting it consists uniquely of a talc-like phase with minor quartz impurities (Fig. 5d).

Under the optical microscope, type IV garnierite consists of yellow to brown, banded, botryoidal aggregates, and is grey to yellow in crossed polars. It is commonly intergrown with, superimposed and/or crosscut by quartz veinlets (Fig. 6d, f). In the samples where type IV forms rounded granules, the saprolite fragments are coated by botryoidal garnierite, and this in turn is enveloped by the microcrystalline quartz matrix (Fig. 6g). This matrix is formed by equigranular rounded quartz grains of about 0.1 mm accompanied by disaggregated, angular, talc-like fragments up to 0.5 mm long, which are dark brown under plane polarised light and grey to orange under crossed polars (Fig. 6g, h). The banded aggregates are often fractured and crosscut by quartz veinlets of up

to 0.1 mm thick, and may show microscopic shearing (Fig. 6h). These features suggest that type IV and microcrystalline quartz precipitated from a colloidal silica gel, while the saprolite clasts are interpreted as relicts. The X-ray diffraction patterns and textures of the type IV garnierite are similar to those reported for garnierites from New Caledonia (e.g. sample G6, Figs. 7 and 9 in Wells *et al*., 2009).

4.6. Type V garnierite (Ni-sepiolite-falcondoite)

Ni-sepiolite and falcondoite form white to pale green compact sets of schistose, friable, soft material (Fig. 4h, i). These textures are easily distinguishable from those observed in the other garnierites described above (see Tauler *et al*., 2009 for a detailed study). Ni-sepiolite also occurs as fibrous aggregates embedded in a microcrystalline quartz matrix, which appear as silicified clasts in garnierite-cemented breccias in Figure 4d.

5. Mineral chemistry of garnierites

5.1. Structural formulae

Microprobe chemical analyses of the described garnierite types are summarized in Table 2. The structural formulae were calculated on the basis of 7 oxygens for serpentine and serpentine-like phases (saprolite serpentine, garnierite types I and II), and of 11 for talc-like phases (type IV). Analyses of type III were calculated assuming 7 and 11 oxygens, because their XRD patterns indicate the equally significant presence of both serpentine- and talc-like phases. For sepiolite-falcondoite, calculations were performed using 32 oxygens. In general, oxide totals of the analyses of serpentine- and talc-like garnierites are below the ideal values for these structure types. Most of the studied garnierites are Al-free with only very few having significant Al content. Only saprolite Ni-serpentine and type I garnierite contain Fe, and all the Fe was calculated as Fe^{3+} (Wells *et al.*, 2009). The Fe^{3+} and Al were allocated to the tetrahedral layer until fully occupied (Golightly and Arancibia, 1979). In addition, the fraction of serpentine (X_{serp}) and talc (X_{tlc}) were calculated for garnierite types II and III according to the formulae given by Brindley and Hang (1973).

5.1.1. Saprolite Ni-serpentine

Serpentine from the saprolite has the structural formula of an ideal serpentine, with 2 tetrahedral cations and about 3 octahedral cations. The serpentine is characterised by its

remarkable high Fe content (0.05–0.50 apfu), 0.07–0.24 apfu Ni and variable Al (up to 0.23 apfu). Its average structural formula is $Mg_{2.32}Ni_{0.20}Fe_{0.19}Al_{0.05}Si_{2.00}O_5(OH)_4$. Similar compositional attributes have been reported of the saprolite serpentine from the Loma Ortega 3 deposit in the north western block of the Loma Caribe massif (Gallardo *et al*., 2010b). Talc-like replacements show Ni and Fe contents of 0.81–1.74 and 0.01–0.06 apfu, respectively, with the average structural formula $Mg_{1.88}Ni_{1.08}Fe_{0.04}Si_{4.00}O_{10}(OH)_2 \cdot (H_2O)$.

5.1.2. Type I garnierite

The structural formulae of type I garnierite deviates slightly from that of ideal serpentine with an average cation content of 2.08 apfu in the tetrahedral site and 2.76 apfu in the octahedral site. Comparable results were obtained for the 7 Å-type garnierites by Brindley and Hang (1973). Fe and Ni contents are relatively high (0.07–0.32 and 0.03–0.59 apfu, respectively). Serpentine-like garnierites with a similar Fe content were reported by Wells et al. (2009). The average structural formula of the type I garnierite is $Mg_{2.22}Ni_{0.26}Fe_{0.17}Si_{2.10}O_5(OH)_4$. The Ni content of the spindle-shaped talc-like phase coexisting with type I garnierites is 1.06–2.16 apfu and its structural formula is $Mg_{1.73}Ni_{1.37}Fe_{0.03}Si_{3.92}O_{10}(OH)_2 \cdot (H_2O)$.

5.1.3. Type II garnierite

The structural formulae of type II garnierite differs significantly from ideal serpentine. It has excess of tetrahedral occupancy (2.20 apfu) and an apparent deficit in the octahedral site (2.57 apfu). Similar values have been published for 7 Å-type garnierites by Brindley and Hang (1973) and Wells *et al.* (2009). The garnierite has higher Ni (0.30–1.88 apfu) and lower Fe (up to 0.10 apfu) than type I, and is the only garnierite with remarkable Al content (up to 0.11 apfu). Its average structural formula is $Mg_{1.58}Ni_{0.92}Al_{0.05}Fe_{0.03}Si_{2.17}O_5(OH)_4$, with an average serpentine fraction (X_{serp}) of 0.71. The talc-like fine-grained envelope has a composition of 1.22–3.04 Ni apfu and 0–0.02 Fe apfu, with an average structural formula of $Ni_{2.56}Mg_{0.78}Fe_{0.01}Si_{3.82}O_{10}(OH)_2 \cdot (H_2O)$.

5.1.4. Type III garnierite

When calculated on the basis of 7 oxygens, the structural formulae of type III garnierite also deviate from the ideal serpentine. It however, has a higher Ni (1.28–2.19 apfu) and lower Fe (up to 0.04 apfu) contents than type II. On the basis of 11 oxygens, it has a

tetrahedral cation deficit and a remarkable octahedral cation excess, and its Ni content ranges between 2.01 and 3.44 apfu. The average structural formula is $Ni_{1.79}Mg_{0.57}Si_{2.31}O_5(OH)_4 \cdot n(H_2O)$ (to 7 oxygens) or $Ni_{2.81}Mg_{0.90}Si_{3.63}O_{10}(OH)_2 \cdot (H_2O)$ (to 11 oxygens), and X_{serp} is 0.53.

5.1.5. Type IV garnierite

The structural formula of the bluish green (type IV) garnierite is similar to that of ideal talc-willemseite, but the EMP analyses show low oxide totals. The brown botryoidal aggregates show a wide range of Ni concentrations (0.89–2.83 apfu) as well as the lowest Fe contents. Its average structural formula is $Mg_{1.56}Ni_{1.53}Si_{3.94}O_{10}(OH)_2 \cdot (H_2O)$. The brown fragments in the microcrystalline quartz matrix have the structural formula $Ni_{2.18}Mg_{0.94}Al_{0.01}Si_{3.92}O_{10}(OH)_2 \cdot (H_2O)$ and slightly higher Ni contents (2.12–2.22 apfu) and similar Fe content (up to 0.03 apfu) compared to the coexisting brown botryoidal aggregates.

5.1.6. Type V garnierite (Ni-sepiolite-falcondoite)

The composition of Ni-sepiolite and falcondoite is characterized by 0.34–5.24 apfu Ni and very low Al and Fe contents. Their average structural formula is $Mg_{5.76}Ni_{1.69}Si_{12.22}O_{15}(OH)_2 \cdot 6(H_2O)$.

5.2. X-ray element mapping

A detailed study of quantified X-ray element maps shows the relationships between textural position, sequence of crystallization and mineral composition of the various garnierite samples. In order to examine the distribution of major element in the different garnierites, the elements Si, Mg, Ni, Fe and Al were scanned in four selected areas containing saprolite serpentine (Fig. 7), serpentine-like, talc-like garnierites and their mixture (Fig. 8), talc-like garnierite (Fig. 9), and sepiolite-falcondoite (Fig. 10). The element maps show a complex and variable texture and mineral composition. Note that there is a close fit between spot analyses (section 5.1) and quantified pixel compositions (this section). The subtle divergences are the result of matrix effects (for these plots a single internal standard was used for all minerals of the scanned areas).

The textural and compositional features of saprolite serpentine are presented in Fig. 7. The map shows a mesh texture in which Fe oxyhydroxide aggregates (brown areas in

Fig. 7b) are wrapped by Fe-bearing, Ni-poor serpentine, and this in turn is surrounded by serpentine with higher Ni. This indicates replacement of the primary olivine by the secondary saprolite serpentine (Ni-enriched), as the Ni-rich solution percolated through small fractures and discontinuities. In addition, a Ni-poor serpentine is also found in a vein, showing lower Fe and higher Al than the saprolite serpentine, similar to those of the oceanic hydrothermal serpentine.

The distribution of elements in talc-like, serpentine-like, intermediate phase and quartz are presented in Figure 8, and a detail of talc-like is shown in Figure 9. The texture of the talc-like phase is complex, characterised by an oscillatory banded, botryoidal fabric, suggesting several stages of talc-like growth. These bands present strong variations in the Ni content, pointing to recurrent changes in the physical-chemical conditions in the aqueous medium during garnierite formation. However, the quantified XR maps suggest two compositional maxima for this talc-like phase, as shown in Figs. 8a and 9a. Voids and fractures are later filled by microcrystalline quartz. This quartz contains small amounts of Ni. This phase represents a poorly defined variety of Ni-bearing, microcrystalline quartz, probably chrysoprase (Fig. 8b). In Figure 8c it is also evident the post-depositional diffusion transport of Fe from relictic (saprolite) serpentine within adjacent talc. To be noted also is the presence of a phase with a homogeneous intermediate composition between talc- and serpentine-like, comparable to that of karpinskite, which stands out clearly in the images associated with serpentine. This is confirmed by the quantified Si/(Mg+Fe+Ni) image (Fig 8c), that shows the correspondence between the theoretical values of this ratio in stoichiometric serpentine (0.67) and karpinskite (1.00) and the quantified pixels of both minerals. According to the triangular plot in Figure 8e, some spot and pixel analyses located in between major clusters represent mixtures of minerals. However, a small cluster located midway in between talc and serpentine corresponds to the area identified as karpinskite in the quantified XR maps. Note that this cluster plots in the line representing the solid solution of karpinskite.

As seen in Figure 10, the textural and chemical variations suggest three stages of sepiolite crystallization, starting with homogeneous Ni-poor sepiolite aggregates, followed by Ni-rich sepiolite. In the last stage still Ni-richer sepiolite crystallized along fractures and/or channels. This progressive Ni enrichment in sepiolite was also observed by Tauler *et al*. (2009). Quartz crystallized in the wall of voids, within the matrix of

sepiolite, and locally along fractures/channels. Ni-rich regions in quartz are noted at the rims of the quartz grains related to the third stage of Ni-rich sepiolite growth.

5.3. The Si-Mg-Ni system

All analyses performed on garnierite types I-IV, Ni-sepiolite-falcondoite (including results from Tauler *et al.*, 2009) and saprolite serpentine are represented in the Si-Mg-Ni system in Fig. 11a-c, and compared with analyses of garnierites from other localities provided by other authors, shown in Figure 11d. In general, the analysed garnierites plot within the field limited by sepiolite-falcondoite and lizardite-népouite series. Serpentine and serpentine-like minerals with lower Ni and higher Fe concentrations (serpentine from saprolite and type I garnierite) plot near the lizardite end member. Type II display intermediate Ni compositions between type I and III. Analyses of type I, II and III plot closer to the kerolite-pimelite series as they are richer in Ni. Some type I and II, and all type III garnierites plot close to the 50% Si line (Si/(Mg+Fe+Ni) = 1). The analyses of brown botryoidal aggregates of type IV plot continuously in a wide range of compositions between the kerolite-pimelite end members (Fig. 11b). Figure 11b also shows that the brown fragments in the microcrystalline quartz matrix have higher Ni contents than the brown botryoidal aggregates they coexist with; and that the talc-like replacements of saprolite fragments and spindle-shaped, talc-like, fine grained envelope in type II have similar compositions to those of type IV garnierite. The Ni-sepiolite-falcondoite analyses also plot continuously between sepiolite and falcondoite end members (Fig. 11c). The sepiolite analyses are, however, slightly enriched in Si probably due to microscopic intergrowths of quartz within sepiolite (Tauler et al., 2009). These results suggest the existence of a complete solid solution between Mg and Ni end members.

In general, Ni-Mg hydrous silicates from Falcondo Mine have similar structural and chemical characteristics to garnierite minerals examined in other worldwide Ni-lateritic deposits (Fig. 11d), except for the Ni-dominant serpentine-like phases, which have not been recorded in Falcondo, and falcondoite, which commonly occurs in this deposit.

6. Discussion

6.1. Garnierite mineralisation and brittle tectonic structures

In general, unweathered serpentinised peridotites are massive and do not allow fluids to circulate except along fractures (Genna *et al.*, 2005; Cluzel and Vigier, 2008). The creation of open spaces enables water circulation and Ni mobility, thus fracturing and faulting promotes weathering and preferential Ni concentration. Garnierite mineralisations follow previous structures such as joints and shear zones in serpentinised peridotites (Freyssinet *et al.*, 2005). Ore thickness, grade and type of Ni-laterite deposits are controlled by fractures, faults and shear zones in bedrock and regolith (Leguéré, 1976; Butt and Cluzel, 2013). Unfortunately, little attention has been placed on the effect of brittle tectonics on the formation of garnierites (Cluzel and Vigier, 2008).

In the Falcondo Ni-laterite deposit, evidences of garnierite precipitation during deformation are common. Striations on coated fault surfaces (Fig. 3k, l) and fault breccias containing garnierite clasts cemented by garnierite (Fig. 4d), indicate that the precipitation of the ore minerals was synchronous with brittle tectonics affecting the evolving weathering profile. Haldemann et al. (1979) and Mann et al. (1991) considered these types of faults as evidence of continuous tectonic uplift since at least the Miocene. The tectonic uplift controlled much of the evolution of the profile by allowing the exposure of deeper levels concomitant with erosion at the surface. Cluzel and Vigier (2008) documented similar relationships between brittle tectonics and synchronous precipitation of garnierites in the New Caledonian lateritic weathering profile

Although the majority of garnierite mineralisations in the Falcondo deposit occur as infillings and coatings on fracture surfaces, their textures/structures suggest they precipitated in an active tectonic environment. The fault structures in which garnierites precipitated were formed during uplift and weathering of the serpentinised peridotite body. Thus, garnierite-containing fractures hosted in unweathered protolith (Fig. 3d) document tectonic rupture and uplift of the country ultramafic rock before it could be altered to saprolite, suggesting rapid uplift tectonics compared to weathering rates. Also, the botryoidal habit of type IV garnierite (Fig. 4g), which represent precipitation from a colloidal solution in open spaces, are commonly fractured and brecciated (Fig. 4g, h), and the fragments are cemented by a second generation of garnierite and rounded quartz grains. These textures suggest multiple precipitation and deformation events, which may explain the origin of the bimodal composition of the botryoidal talc-like phase (Figs. 8 and 9). Similarly, garnierite clasts within breccias (Fig. 4d) indicate a

mineralisation stage prior to a brittle deformation. The fracturing formed tectonic porosity that enhanced the circulation of solutions and the precipitation of a second generation of garnierite, namely type III.

In summary, our observations suggest a regional syn-tectonic environment for the generation of the Ni-ore garnierite deposits in Falcondo, even if the precipitates are pre-, syn- or post-kinematic with respect to the activity of a particular fault. This brittle syn-tectonic environment has played an important role in the formation of hydrous silicate Ni-laterites, since it triggered cyclic, recurrent processes of weathering and erosion. These processes allowed the draining of fluids and reworking of previously formed ore, thus favouring remobilisation and reconcentration of ore minerals.

6.2. Garnierites and garnierites

Different greenish colours have been observed in the garnierite samples, which correspond to different mineral assemblages as demonstrated by XRD and EMP analyses. The various phases have been classified as type I to V garnierites. These garnierites show characteristic patterns of serpentine-like (type I), talc-like (type IV) and sepiolite-like minerals (type V). Also, mix phases with different proportion of serpentine- and talc-like phases (types II and III) are also common. The different colours of the studied garnierites (Fig. 3) are not an indication of the Ni content in the minerals as shown in Figure 11. This is contrary to the observation of Brindley and Hang (1973). However, in the sepiolite-falcondoite series, the greenness of the sample is directly correlated with the Ni concentration. The characteristic colour of type I to IV garnierites gives information on the dominant mineral phase present in the sample (serpentine-like, talc-like or mixtures), which is useful for a field mineral identification with the naked eye.

The following sections illustrate the complex mineralogical and compositional relations of garnierites. First, saprolite serpentine and type I serpentine-like garnierite compositions mainly display a lizardite [$Mg_3Si_2O_5(OH)_4$] stoichiometry (Fig. 11a). Deviations from the lizardite-népouite line toward the kerolite-pimelite line (types II and III) are due to mixing or interstratifications of 1:1 and 2:1 layers to form a mix phase (Faust, 1966; Vitovskaya and Berkhin, 1968, 1970). According to Brindley and Hang (1973), however, the same observations can be interpreted as deficiencies of octahedral cations in the 7 Å-type and of tetrahedral cations in the 10 Å-type garnierites.

These mixtures (type II and III) show similar tetrahedral versus octahedral cation (T/O) ratios to that of the intermediate series karpinskite-Ni-karpinskite (T/O = 1; Figs. 8e and 11a). However, the existence of karpinskite as a mineral species is debatable. Although EMP analyses and XR-maps show discrete homogenous regions with a composition similar to karpinskite, its presence is not supported by the X-ray diffractograms. More work is required in order to validate its existence.

Second, the type IV (talc-like) and type V (sepiolite-like) garnierites cover a wide range of composition and plot near the kerolite [$Mg_3Si_4O_{10}(OH)_2 \cdot (H_2O)$]-pimelite [$Ni_3Si_4O_{10}(OH)_2 \cdot (H_2O)$] and sepiolite [$Mg_4Si_6O_{15}(OH)_2 \cdot 6(H_2O)$]-falcondoite [$Ni_4Si_6O_{15}(OH)_2 \cdot 6(H_2O)$] lines respectively. The observed excess in Si in sepiolite-falcondoite series (Fig. 11c) may be due to a true excess of Si in the octahedral site or to contamination of microscopic silica rods, as reported by Tauler *et al.* (2009).

As pointed out by many authors and summarized by Galí *et al.* (2012), the results of this study suggest complete miscibility along the lizardite-népouite, kerolite-pimelite and the sepiolite-falcondoite lines under atmospheric conditions temperature. However, few data exist on the mechanism of Ni-Mg substitution in Ni-phyllosilicates (Manceau and Calas, 1985). The distribution and speciation of nickel has been studied in saprolite serpentine from New Caledonia (Dublet et al., 2012) and the Philippines (Fan and Gerson, 2011), in lizardite-népouite and kerolite-pimelite from New Caledonia (e.g. Manceau and Calas, 1985), and in Ni-sepiolite from the Dominican Republic (Roqué-Rosell *et al.*, 2011). EXAFS (Extended X-ray Absorption Fine Structure) results suggest a heterogeneous distribution of Ni in the octahedral sheets of the Ni-phyllosilicates, forming discrete domains (clustering). In addition, Dublet *et al*. (2012) reported that Ni is randomly distributed in the Ni-serpentines from the bedrock (peridotite) and clustered in the Ni-serpentines from saprolite. Further XAS (X-ray Absorption Spectroscopy) is needed to define the mechanism of Ni-Mg substitution in garnierite minerals.

The low oxide totals observed in talc-like garnierite can be explained by the presence of excess water, which may occupy interlayer positions in a 10 Å-type structure, as suggested by Brindley et al. (1979). Hence, we consider that for this type of phase, the terms *kerolite* and *pimelite* are more appropriate than talc and willemseite. Although kerolite and pimelite are not accepted as mineral species by the IMA, they have been described in other laterite deposits, for example in New Caledonia (e.g. Wells *et al.*,

2009; Dublet *et al.*, 2012), Poland (e.g. Wiewióra, 1978; Dubińska *et al.*, 2000) and India (e.g. Som and Joshi, 2002). In addition, in the Cerro Matoso in Colombia Ni-laterite, pimelite is one of the main garnierite-forming minerals (Lopez-Rendon, 1986; Gleeson *et al*., 2004). Also, kerolite has been reported in other settings including karst environments (e.g. Ducloux *et al.*, 1993), palustrine-lacustrine (e.g. Martín de Vidales *et al.*, 1991; Pozo and Casas, 1999) and in oceanic sediments (e.g. Cole and Shaw, 1983). Therefore, kerolite and pimelite are important components in not only hydrous silicate Ni-laterites but in other deposits worldwide.

The lack of iron is a chemical characteristic of garnierite minerals (Troly *et al*., 1978). Manceau and Calas (1985) suggested that serpentine-like garnierites may have small amounts of iron (systematically below 1.5 wt.% Fe_2O_3), compared to talc-like garnierites, which are iron-free. It is generally accepted that the lack (or very low content) of iron confirms the secondary (neoformed) origin of garnierites, since Fe is largely not soluble under common weathering conditions. In the case of Falcondo, all garnierites fulfil this condition except type I, which display significant Fe values (1.8–6.8 wt.% Fe_2O_3) similar to those of saprolite serpentine (1.5–8.6 wt.% Fe_2O_3). This observation indicates that neoformed serpentine-like garnierite of the lateritic profile can be Fe-rich. In the Falcondo deposit, this Fe-bearing Ni-phyllosilicate was the first garnierite to be precipitated.

In the Falcondo deposit, the predominant garnierite is kerolite-pimelite (type IV), the 10 Å phase, having one of the highest Ni contents (up to 2.83 apfu). Also, Falcondo is the only locality in the world where the Ni-dominant sepiolite (falcondoite) occurs (Springer, 1976; Tauler et al., 2009). However, the Ni-dominant serpentine (népouite) has not been described yet. Possibly it only occurs as a mixture with Ni-kerolite-pimelite at the nanoscale. Mixtures of lizardite-népouite and kerolite, and of lizardite-népouite and smectite are also described in New Caledonia (Fig. 20 in Pelletier, 1996; Wells *et al*., 2009). In contrast, in New Caledonia, the presence of a serpentine-like (népouite) garnierite is well documented (e.g. Glasser, 1907; Maksimović , 1973; Brindley and Wan, 1975). The difference among these two Ni-laterite localities may be explained by the lithology of the primary ultramafic rocks. In New Caledonia, the protolith is mainly harzburgite and dunite (e.g. Troly *et al.*, 1979; Pelletier, 1983, 1996; Perrier *et al*., 2006; Dublet *et al*., 2012) and lherzolite is rare (Cluzel *et al.*, 2012), whereas in the Dominican Republic the protolith is mostly clinopyroxene-rich

harzburgite and lherzolite (e.g. Marchesi *et al.*, 2012). The higher content in pyroxenes suggests higher activity of silica in the Dominican than in the New Caledonian, leading to the preferential formation of talc rather than serpentine during weathering.

6.3. Origin of Falcondo garnierites

Similar to other hydrous silicate-type laterites, the Falcondo deposit in the Dominican Republic was formed by tropical weathering of ultramafic rocks undergoing continuous tectonic uplift. Coupled with a low water table, these conditions resulted in the development of a thick saprolite horizon, and a thin ferruginous oxide horizon (Golightly, 1981; Brand *et al*., 1998; Elias, 2002; Gleeson *et al*., 2003; Lewis *et al*., 2006; Butt and Cluzel, 2013).

During laterisation, the main Ni-containing primary silicates are altered to secondary phases which are more stable under the oxidising ambient conditions. Under these conditions, Mg contained in the primary ferromagnesian silicate minerals is solubilised and leached out of the weathering profile. Ferrous Fe originally contained in the silicates is oxidised to the insoluble Fe^{3+}, which is residually concentrated as goethite in the limonite horizon. The Ni released from the silicates is retained in goethite. The retention of Fe in the limonite explains the low Fe content of the garnierites in the Falcondo deposit (Tauler et al., 2009; and references therein). The Ni in goethite from the limonite may subsequently be leached by percolating acidic solutions to deeper levels in the profile where it may be co-precipitated with hydrous Mg silicates around water table (e.g. Avias, 1978; Trescases, 1979; Golightly, 1981; Brandt et al., 1998; Freyssinet 2005). This interpretation is supported by the negative correlation of Mg with Ni and Fe in saprolite serpentines, where Ni increases more rapidly than Fe (Golightly and Arancibia, 1979). The Fe in saprolite serpentines is residual, and the Ni is imported from the upper lateritic levels (Trescases, 1973, 1979; Avias, 1978). The Ni is incorporated first in the saprolite Ni-bearing serpentines (Pelletier, 1996). Once the Ni-serpentines are saturated, the excess Ni is precipitated as hydrous Mg silicates (garnierites) in open spaces including cracks and faults. The precipitation is caused by a sudden change in Eh/pH of the solution. The high stability of the octahedrally coordinated Ni^{2+} ion (Burns, 1970) favours the formation of nickeliferous trioctahedral phyllosilicates (e.g. Trescases, 1975).

In general, the stability of Ni-bearing minerals in lateritic environments is determined by the Eh, pH, and chemical composition of permeating groundwater (e.g. Trescases, 1973). In an Al-free system, such as in the Falcondo profile, the stability of lizardite-népouite, kerolite-pimelite or sepiolite-falcondoite is controlled by the silica activity (Galí *et al.*, 2012). The ideal formation of the Ni ore occurs as a succession of precipitation of mineral phases progressively enriched in Ni and with higher Si, because silica activity increases with time and through the profile. Thus, the first garnierite to precipitate is lizardite-népouite, followed by kerolite-pimelite, sepiolite-falcondoite and Ni-free sepiolite with quartz (Galí *et al.*, 2012). This mineral sequence is coherent with field observations and textural relationships between types I-II and type IV. In this mineral sequence the silica activity increases progressively, as well as pH decreases and Eh becomes more oxidising (Golightly, 1981; Golightly, 2010; Gleeson *et al*., 2004). In alkaline conditions (pH > 8) garnierite minerals are the least-soluble Mg-Ni phyllosilicates, whereas at lower pH quartz may precipitate. The occurrence of later quartz indicates subsequent acidification conditions as a result of rapid access of meteoric surface waters (acidic) to deeper levels (e.g. Golightly, 1981).

According to our results, the first supergene Ni-phyllosilicate phase that was formed in the Falcondo deposit was an Fe-bearing, nickel-enriched, serpentine-like garnierite (type I). Its Fe content is similar to that of saprolite serpentine and suggests that type I garnierite precipitated in a Ni-saturated, rock-dominated system under more alkaline and reducing conditions. On the other hand, the other types of garnierite (type II-V) were precipitated under conditions in which Fe was insoluble as suggested by their low Fe content. Furthermore, the mix serpentine- and talc-like phases (types II and III) may have precipitated under an intermediate stage between the stability fields of Ni-serpentine and kerolite-pimelite (see Fig. 6 in Galí *et al*., 2012). These interpretations are coherent with the textures observed in the Falcondo garnierites, where talc-like phases frequently envelop type I and II garnierites (Fig. 4a, b), and the remaining porosity is finally filled by quartz and/or silica. In the particular case of Falcondo, the mineral sequence is more complex. For example, the polyphase infilings containing serpentine- and talc-like garnierite shown in Figure 4a, b suggest that the conditions of the system allowed the formation of serpentine- followed by talc-like phases in the same vein, when the fracture was open. Also, textural-chemical features revealed by the X-ray maps indicate several stages of growth with strong oscillatory changes in Ni content

in type IV (Figs. 8 and 9), and progressive Ni enrichment in type V (Fig. 10). These observations point to recurrent variations in the physical-chemical conditions during garnierite precipitation-dissolution in an aqueous medium.

6.4. Metallurgical implications

Variations in the chemical composition of garnierites imply changes in the behaviour of the laterite ore during mineral processing. The laterite ore is a mixture composed mainly of Ni-bearing saprolite serpentine with variable amounts of garnierite, Fe-oxyhydroxides from the limonite horizon, and fresh, unserpentinised and serpentinised peridotite. Due to the high water content of the laterite ore, in the form of free moisture or combined as hydroxyl/molecular water in the mineral structures, it must be first dehydrated by calcination at about 900ºC. The calcination product is later briquetted and partly reduced to transform Ni and Fe oxides into metallic Ni and Fe in the solid state. The ore is then smelted to form a slag at about 1600ºC in an electric furnace in the presence of carbon (Dalvi *et al*., 2004; and references therein).

The garnierites characterised in this paper present different water contents. Judging from the mass deficiency of the EPM analyses, the H_2O contents are about 15 wt.% in the serpentine-like (garnierite types I and II, also in saprolite serpentine, the main component of the laterite ore), 11 wt.% in garnierite mixtures (type III), 10 wt.% in the "hydrated" talc-like (type IV) and 17 wt.% in the sepiolite-like (type V).

In the case of Falcondo, in order to produce ferronickel containing ca. 40% nickel and 60% iron, operation in a conventional electric furnace requires high SiO_2/MgO ratios (~2; wt.% units) and low FeO (~20 wt.% FeO) (Dalvi *et al*., 2004). This ratio acts as a flux in the smelting process. Thus a low SiO_2/MgO leads to an increase of the temperature in the furnace, and to higher energy consumption. The garnierite typologies reported in Falcondo display different SiO_2/MgO ratios: the highest average silica/magnesia is found in types III (6.5), IV (4.6) and V (3.2), followed by type II (2.3) and type I (1.5). The ratio of type I is similar to that of saprolite Ni-serpentine (1.5). In addition, in all cases, the Ni content and the SiO_2/MgO ratio correlate fairly well because Ni substitutes for Mg in the octahedral position. As a result, processing ore containing remarkable amounts of type III or IV garnierites (with relatively high Si and Ni, thus high SiO_2/MgO ratios) requires a lower temperature than processing saprolite

serpentine with or without serpentine-like garnierites (with less Si than type III and IV and lower Ni, thus low SiO_2/MgO ratios).

In summary, these variations in water content, Ni and SiO_2/MgO ratio should be taken into account for the preparation of the laterite ore mixture prior to calcination and smelting. Therefore, an accurate mineralogical characterisation of garnierite-forming minerals is important from a metallurgical point of view.

7. Conclusions

This article synthesises previous information and provides new data on the mode of occurrence, mineralogy and mineral chemistry of the garnierites from the Falcondo Ni-laterite deposit in the Dominican Republic. The following are some important conclusions from this study:

1. The garnierites in the Falcondo weathering profile were precipitated in a tectonically active regime in which Ni was reconcentrated through recurrent weathering-uplift-erosion cycles. In some cases, the precipitation was syn-kinematic.

2. The garnierites in the Falcondo weathering profile occur in various shades of greenish colour which, in addition to textural features, characteristic XRD patterns and chemical composition, have been used to classify them into five groups. The end member phases identified include serpentine-like, talc-like, and sepiolite-like phases. In addition, intermediate phases with mixed serpentine- and talc-like end members were also observed and interpreted as mixtures at nano scale. The mole fractions of the end members in the mixed phases were calculated from EMP analyses. XR element maps showed complex textures and variable compositions. It is worth noting that the intensity of the greenish colour is not a direct indicator of the Ni amount in the sample (except for sepiolite-falcondoite series), but gives information on the dominant mineral phase present in the garnierite.

3. The formation of the ore occurred in successive stages becoming progressively enriched in Ni and Si. The precipitation sequence was as follows: iron-bearing Ni-enriched serpentine (Type I), iron-free mixtures between serpentine and kerolite-pimelite (types II and III), kerolite-pimelite (type IV), and sepiolite-falcondoite (type V), being quartz the final product.

4. The talc-like phase (10 Å-type), which shows one of the highest Ni contents, is the dominant garnierite phase in the profile. This contrasts with the New Caledonian Ni-laterites, where the serpentine-like garnierite is the most common phase. This difference is probably due to the lower silica activity in the profile imposed by a harzburgite/dunite protolith, as opposed to a clinopyroxene-rich harzburgite/lherzolite protolith in the Loma Caribe peridotite.

5. The wide variation in the garnierite mineralogy has important implication on ore processing due to variation in the SiO_2/MgO ratio which requires careful blending before feeding the ore into the smelter.

Acknowledgements

This research has been financially supported by the Spanish projects CGL2009-10924 and CGL2012-36263, the Catalan project SGR 2009-444, and a PhD grant to CVdB sponsored by the Ministerio de Educación (Spain). The help and hospitality extended by the staff at Falcondo Glencore mine, in special by Giovanni Bloise, are sincerely acknowledged, as well as the technical support in EMP sessions by Dr. X. Llovet. The authors are also grateful to M.A. Wells and to an anonymous reviewer for their careful and exhaustive revision, which improved enormously the quality of the manuscript. We also thank T. Aiglsperger for figures 1 and 3a.

References

Avias, J., 1968. L'évolution des idées et des connaissances sur la genèse et sur la nature des minerais de nickel, en particulier latéritiques, de leur découverte à nos jours. Bull. BRGM sec. II, 3, 165-172.

Bence, A.E., Albee, A.L., 1968. Empirical correction factors for the electron microanalysis of silicates and oxides. J. Geol. 76, 382-403.

Bowin, C.O., 1966. Geology of the central Dominican Republic (a case history of part of an island arc). In: Hess, H. (Ed.). Caribbean Geological Studies. Geol. Soc. Am., Mem. 98, 11-84.

Brand, N.W., Butt, C.R.M., Elias, M., 1998. Nickel laterites: classification and features. AGSO J Australian Geol. & Geophys. 17(4), 81-88.

Brindley, G.W., 1978. The structure and chemistry of hydrous nickel containing silicate and aluminate minerals. Bull. BRGM sec. II, 3, 233-245.

Brindley, G.W., 1980. The structure and chemistry of hydrous nickel-containing silicate and nickel-aluminium hydroxy minerals. Bull. Miner. 103, 161-169.

Brindley, G.W., Bish, D.L., Wan, H.M., 1979. Compositions, structures, and properties of nickel-containing minerals in the kerolite-pimelite series. Am. Miner. 64, 615-625.

Brindley G.W., Hang P.T., 1973. The nature of garnierite: I. Structure, chemical compositions and color characteristics. Clay. Clay Miner. 21, 27-40.

Brindley, G.W., Maksimović, Z., 1974. The nature and nomenclature of hydrous nickel-containing silicates. Clay Miner. 10, 271-277.

Brindley, G.W., Wan, H.-M., 1975. Compositions, structures and thermal behaviour of nickel-containing minerals in the lizardite-népouite series. Am. Miner. 60, 863-871.

Butt, C.R.M., Cluzel, D., 2013. Nickel laterite ore deposits: weathered serpentinites. Elements 9, 123-128.

Burns, R.G., 1970. Mineralogical Applications of Crystal Field Theory. Cambridge University Press, United Kingdom, pp. 551.

Caillère, S., 1965. Composition minéralogique des differents types de minerais de nickel de la Nouvelle-Calédonie. Mém. Muséum National Hist. Nat. 12, 105-124.

Cluzel, D., Maurizot, P., Collot, J., Sevin, B., 2012. An outline of the Geology of New Caledonia; from Permian-Mesozoic Southeast Gondwanaland active margin to Cenozoic obduction and supergene evolution. Episodes 35, 72-86.

Cluzel, D., Vigier, B., 2008. Syntectonic mobility of supergene nickel ores of New Caledonia (Southwest Pacific). Evidence from garnierite veins and faulted regolith. Resour. Geol. 58, 161-170.

Cole, T.G., Shaw, H.F., 1983. The nature and origin of authigenic smectites in some recent marine sediments. Clay Miner. 18, 239-252.

Dalvi, A.D., Gordon Bacon, W., Osborne R.C., 2004. The past and the future of nickel laterites. PDAC Int. Convention (March 2004). Proceedings PDAC 2004. Prospectors and Developers Association of Canada, Toronto, Canada, p. 27.

DeWaal, S.A., 1970. Nickel minerals from Barberton, South Africa: III. Willemseite, a nickel-rich talc. Am. Miner. 55, 31-42.

Draper, G., Gutiérrez, G, Lewis, J.F., 1996. Thrust emplacement of the Hispaniola peridotite belt: Orogenic expression of the mid-Cretaceous Caribbean arc polarity reversal? Geology 24, 1143-1146.

Dubińska, E., Sakharov, B.A., Kaproń, G., Bylina, P., Kozubowski, J.A., 2000. Layer silicates from Szklary (Lower Silesia): from ocean floor metamorphism to continental chemical weathering. Geol. Sudetica 33, 85-105.

Dublet, G., Juillot, F., Morin, G., Fritsch, E., Fandeur, D., Ona-Nguema, G., Brown Jr., G.E., 2012. Ni speciation in a New Caledonian lateritic regolith: a quantitative X-ray absorption spectroscopy investigation. Geochim. Cosmochim. Acta 95, 119-133

Ducloux, J., Boukili, H., Decarreau, A., Petit, S., Perruchot, A., Pradel, P., 1993. Un gîte hydrothermal de garniérites: l'exemple de Bou Azzer, Maroc. Eur. J. Mineral. 5, 1205-1215.

Elias, M., 1981. Geology, Mineralogy, and Chemistry of Lateritie Nickel-Cobalt Deposits near Kalgoorlie, Western Australia. Econ. Geol. 76, 1775-1783.

Elias, M., 2002. Nickel laterite deposits—Geological overview, resources and exploration. In: Cooke, D., Pongratz, J., (Eds.). Giant ore deposits—Characteristics, genesis, and exploration. CODES Special Publication 4, University of Tasmania, Hobart, pp. 205–220.

Escuder-Viruete, J., Pérez-Estaún, A., Contrera, F., Joubert, M., Weis, D., Ullrich, T.D., Spadea, P., 2006. Plume mantle source heterogeneity through time: insights from the Duarte Complex, Hispaniola, northeastern Caribbean. J. Geophys. Res. 112, B04203.

Esson, J., Carlos, L., 1978. The occurrence, mineralogy and chemistry of some garnierites from Brazil. Bull. BRGM sec. II, 3, 263-274.

Fan, R., Gerson, A.R., 2011. Nickel geochemistry of a Philippine laterite examined by bulk and microprobe synchrotron analyses. Geochim. Cosmochim. Ac. 75, 6400-6415.

Faust, G.T., 1966. The hydrous nickel-magnesium silicates – the garnierite group. Am. Mineral. 51, 33-36.

Freyssinet, Ph., Butt, C.R.M., Morris, R.C., 2005. Ore-forming processes related to lateritic weathering. Econ. Geol. 100th Anniversary Vol., 681-722.

Galí, S., Soler, J.M., Proenza, J.A., Lewis, J.F., Cama, J., Tauler, E., 2012. Ni-enrichment and stability of Al-free garnierite solid-solutions: a thermodynamic approach. Clay. Clay Miner. 60, 121-135.

Gallardo, T., Chang, A., Tauler, E., Proenza, J.A., 2010a. El yacimiento de San Felipe (Camagüey, Cuba): un ejemplo de lateritas niquelíferas tipo arcilla. Macla 13, 87-88 (in Spanish).

Gallardo, T., Tauler, E., Proenza, J.A., Lewis, J.F., Galí, S., Labrador, M., Longo, F., Bloise, G., 2010b. Geology, mineralogy and geochemistry of the Loma Ortega Ni laterite deposit, Dominican Republic. Macla 13, 89-90.

García-Casco, A., 2007. Magmatic paragonite in trondhjemites from the Sierra del Convento mélange, Cuba. Am. Mineral. 92, 1232-1237.

Genna, A., Maurizot, P., Lafoy, Y., Augé, T., 2005. Contrôle karstique de minéralisations nickélifères de Nouvelle-Calédonie. C.R. Acad. Sci. II A 337, 367-374.

Gerard, P., Herbillon, A.J., 1983. Infrared studies of Ni-bearing clay minerals of the kerolite–pimelite series. Clay. Clay Miner. 31, 143-151.

Glasser, E., 1907. Note sûr une espèce minérale nouvelle: la népouite, silicate hydraté de nickel et de magnésie. Bull. Soc. Fr. Miner. 30, 17-28.

Gleeson, S.A., Butt, C.R., Elias, M., 2003. Nickel laterites: A review. SEG Newsletter 54, 11-18.

Gleeson, S.A., Herrington, R.J, Durango, J., Velásquez, C.A., Koll, G., 2004. The mineralogy and geochemistry of the Cerro Matoso S.A. Ni laterite deposit, Montelíbano, Colombia. Econ. Geol. 99, 1197-1213.

Golightly, J.P., 1979. Geology of Soroako nickeliferous laterite deposits. Int. Laterite Symposium 3, 38-55.

Golightly, J.P., 1981. Nickeliferous laterite deposits. Econ. Geol. 75th Anniversary Vol., 710-735.

Golightly, J.P., 2010. Progress in understanding the evolution of nickel laterites. Econ. Geol. Spec. Pub. 15, 451-485.

Golightly, J.P., Arancibia, O.N., 1979. The chemical composition and infrared spectrum of nickel- and iron-substituted serpentine from a nickeliferous laterite profile, Soroako, Indonesia. Can. Miner. 17(4), 719-728.

Haldemann, E.G., Buchan, R., Blowes, J.H., Chandler, T., 1979. Geology of lateritic nickel deposits, Dominican Republic. Int. Laterite Symposium 4, 57-84.

Kato, T., 1961. A study on the so-called garnierite from New-Caledonia. Mineral. J. 3, 107-121.

Kato, T., 2005. New accurate Bence-Albee a-factors for oxides and silicates calculated from the PAP correction procedure. Geostand. Geoanal. Res. 29, 83–94.

Kuck, P.H., 2013. Nickel. USGS Mineral Commodity Summaries, 108-109.

Leguéré, J., 1976. Des corrélations entre la tectonique cassante et l'altération supergène des péridotites de Nouvelle Calédonie. PhD Thesis. University of Montpellier, France, 95 pp.

Lewis, J.F., Draper, G., 1990. Geological and tectonic evolution of the northern Caribbean margin. In: Dengo, G., Case, J.E. (Eds.). The Geology of North America, Volume H, The Caribbean region. Geol. Soc. Am., Colorado, pp. 77-140.

Lewis, J.F., Draper, G., Proenza, J.A., Espaillat, J., Jiménez, J., 2006. Ophiolite-Related Ultramafic Rocks (Serpentinites) in the Caribbean Region: A Review of their Occurrence, Composition, Origin, Emplacement and Ni-Laterite Soils Formation. Geol. Acta 4, 237-263.

Lewis, J.F., Escuder-Viruete, J., Hernáiz-Huerta, P.P., Gutiérrez, G., Draper, G., Pérez-Estaún, A., 2002. Geochemical subdivision of the Circum-Caribbean Island Arc, Dominican Cordillera Central: implications for crustal formation, accretion and growth within an intra-oceanic setting. Acta Geol. Hisp. 37, 81-122.

Lewis, J.F., Jiménez, J.G., 1991. Duarte Complex in the La Vega-Jarabacoa-Janico Area, Central Hispaniola: Geological and Geochemical Features of the Sea Floor During the Early Stages of Arc Evolution. In: Mann, P., Draper, G., Lewis, J.F. (Eds.). Geologic and tectonic development of the North America-Caribbean plate boundary in Hispaniola. Geol. Soc. Am. Spec. Paper 262, 115-142.

Lithgow, E.W., 1993. Nickel laterites of central Dominican Republic Part I. Mineralogy and ore dressing. In: Reddy, R.G., Weizenbach, R.N. (Eds.). The Paul E. Queneau Int. Symposium, Extractive Metallurgy of Copper, Nickel and Cobalt, Volume I: Fundamental Aspects. The Minerals, Metals and Materials Society, Portland, pp. 403-425.

Lopez-Rendon, J.E., 1986. Geology, mineralogy and geochemistry of the Cerro Matoso nickeliferous laterite, Cordoba, Colombia. MSc Thesis. Colorado State University, Fort Collins, 378 pp.

Maksimović, Z., 1973. The isomorphous series lizardite-nepouite. Zap. Vses. Mineral. O-va. 102, 143-149 (in Russian).

Manceau, A., Calas, G., 1985. Heterogeneous distribution of nickel in hydrous silicates from New Caledonia ore deposits. Am. Miner. 70, 549-558.

Mann, P., Burke, K., Matumoto, T., 1984. Neotectonics of Hispaniola: plate motion, sedimentation, and seismicity at a restraining bend. Earth Planet. Sc. Lett. 70, 311-324.

Mann, P., Draper, G., Lewis, J.F., 1991. An overview of the geologic and tectonic evolution of Hispaniola. In: Mann, P., Draper, G., Lewis, J.F. (Eds.). Geological and tectonic development of the North American-Caribbean plate boundary in Hispaniola. Geol. Soc. Am. Spec. Paper 262, 1-28.

Marchesi, C., Garrido, C.J., Proenza, J.A., Konc, Z., Hidas, K., Lewis, J.F., Lidiak, E., 2012. Mineral and whole rock compositions of peridotites from Loma Caribe (Dominican Republic): insights into the evolution of the oceanic mantle in the Caribbean region. Geophys. Res. Abs. 14, EGU2012-12161.

Martín de Vidales, J.L., Pozo, M., Alia, J.M., García-Navarro, F., Rull, F., 1991. Kerolite-stevensite mixed-layers from the Madrid Basin, central Spain. Clay Miner. 26, 329-342.

Mudd, G.M., 2010. Global trends and environmental issues in nickel mining: sulfides versus laterites. Ore Geol. Rev. 38, 9-26.

Naganna, C., Phene, S.G., 1968. Study of the nickel silicates associated with the ultrabasic rocks of Nuggihalli schist belt, Mysore state. Proc. Indian Acad. Sci. B 67, 174-179.

Nelson, C.E., Proenza, J.A., Lewis, J.F., López-Kramer, J., 2011. The metallogenic evolution of the Greater Antilles. Geol. Acta 9, 229-264.

Nickel, E.H., Bridge, P.G., 1975. A garnierite with a high nickel content from Western Australia. Mineral. Mag. 40(309), 65-69.

Pecora, W.T., Hobbs S.W., Murata, K.J., 1949. Variations in garnierite from the nickel deposit near Riddle, Oregon. Econ. Geol. 44, 13-23.

Pelletier, B., 1983. Localisation du nickel dans les minerais “garniéritiques” de Nouvelle-Calédonie. In: Nahon, D. (Ed.). Int. Congress on Alteration Petrology, CNRS (Paris, France). Sci. Géol. Mém. 73, 173-183.

Pelletier, B., 1996. Serpentines in nickel silicate ore from New Caledonia. Australasian Institute of Mining and Metallurgy Publication Series - Nickel conference, Kalgoorlie (Western Australia) 6/96, 197-205.

Perrier, N., Ambrosi, J.P., Colin, F., Gilkes, R.J., 2006. J. Biogeochemistry of a regolith: the New Caledonian Koniambo ultramafic massif. Geochem, Explor. 88, 54-58.

Poncelet, G., Jacobs, P., Delannay, F., Genet, M., Gerard, P., Herbillon, A., 1979. Étude preliminaire sûr la localisation du nickel dans une garnierite naturelle. Bull. Miner. 102, 379-385.

Pozo, M., Casas, J., 1999. Origin of the kerolite and associated Mg clays in palustrine-lacustrine environments, the Esquivias Deposit (Neogene Madrid Basin, Spain). Clay Miner. 34, 395-418.

Proenza, J.A., Lewis, J.F., Galí, S., Tauler, E., Labrador, M., Melgarejo, J.C., Longo, F., Bloise, G., 2008. Garnierite mineralisation from Falcondo Ni-laterite deposit (Dominican Republic). Macla 9, 197-198.

Proenza, J.A., Zaccarini, F., Lewis, J., Longo, F. Garuti, G., 2007. Chromite composition and platinum-group mineral assemblage of PGE-rich Loma Peguera chromitites, Loma Caribe peridotite, Dominican Republic. Can. Miner. 45, 211-228.

Roqué-Rosell, J., Villanova-de-Benavent, C., Proenza, J.A., Tauler, E., Galí, S., 2011. Distribution and speciation of Ni in sepiolite-falcondoite- type "garnierite" by EXAFS. Macla 15, 183-184.

Ross, C.S., Shannon, E.V., Gonyer, F.A., 1928. The origin of nickel silicates at Webster, North Carolina. Econ. Geol. 23, 528-552.

Rukavishnikova, I.A., 1956. Some magnesium nickel hydrous silicates of the Nizhne-Tagilsk serpentine massif. Kora Vyvetrivaniya 2, 12-17 (in Russian).

Slansky, E., 1955. Contribution to the knowledge of nickel hydrosilicates from Krems, in southern Bohemia. Universitas Carolina Pragensis Geologica 1, 1-28 (in Czech).

Soler, J.M., Cama, J., Galí, S., Meléndez, W., Ramírez, A., Estanga, J., 2008. Composition and dissolution kinetics of garnierite from the Loma de Hierro Ni-laterite deposit, Venezuela. Chem. Geol. 249, 191-202.

Som, S.K., Joshi, R., 2002. Chemical weathering of serpentinite and Ni enrichment in Fe oxide at Sukinda area, Jajpur district, Orissa, India. Econ. Geol. 97, 165-172.

Song, Y., Moon, H.-S., Chon, H.-T., 1995. New occurrence and characterization of Ni-serpentines in the Kwangcheon area, Korea: Clay Miner. 30, 211-224.

Springer, G., 1974. Compositional and structural variations in garnierites. Can. Miner. 12, 381-388.

Springer, G., 1976. Falcondoite, Ni analogue of sepiolite. Can. Miner. 14, 407-409.

Talovina I.V., Lazarenkov, G.V., Ryzhkova, S.O., Ugol'kov, V.L., Vorontsova, N.I., 2008. Garnierite in nickel deposits of the Urals. Lith. Miner. Res. 43, 588-595.

Tauler, E., Proenza, J.A., Galí, S., Lewis, J.F., Labrador, M., García-Romero, E., Suárez, M., Longo, F., Bloise, G., 2009. Ni-sepiolite-falcondoite in garnierite mineralisation from the Falcondo Ni-laterite deposit, Dominican Republic. Clay Miner. 44, 435-454.

Torres-Roldán, R.L., García-Casco, A., García-Sánchez, P.A., 2000. CSpace: An integrated workplace for the graphical and algebraic analysis of phase assemblages on 32-bit Wintel platforms. Comput. Geosci. 26, 779-793.

Trescases, J.J., 1973. Weathering and geochemical behaviour of the elements of ultramafic rocks in New Caledonia. Bull. Bureau Mineral Resources, Geology and Geophysics, Department of Minerals and Energy 141, 149-161.

Trescases, J.J., 1975. L'évolution géochimique supergène des roches ultrabasiques en zone tropicale: Formation des gisements nickélifères de Nouvelle-Calédonie. Mémoires O.R.S.T.O.M, Paris, 78, pp. 259.

Trescases, J.J., 1979. Remplacement progressif des silicates par les hydroxydes de fer et de nickel dans les profils d'altération tropicale des roches ultrabasiques. Accumulation résiduelle et épigènie. Sci. Geol. Bull. 32, 181-188.

Troly, G., Esterle, M., Pelletier, B., Reibell, W., 1979. Nickel deposits in New Caledonia, some factors influencing their formation. Int. Laterite Symposium 5, 85-119.

Vitovskaya, I.V., Berkhin, S.I., 1968. On the nature of kerolite. Kora Vyvetrivaniya 10, 134-159 (in Russian).

Vitovskaya, I.V., Berkhin, S.I., 1970. On the nature of garnierite. Kora Vyvetrivaniya 11, 26-39 (in Russian).

Wells, M.A., Ramanaidou, E.R., Verrall, M., Tessarolo, C., 2009. Mineralogy and crystal chemistry of garnierites in the Goro lateritic nickel deposit, New Caledonia. Eur. J. Mineral. 21, 467-483.

Whitney, D.L., Evans, B.W., 2010. Abbreviations for names of rock-forming minerals. Am. Miner. 95, 185-187.

Wiewióra, A., 1978. Ni-Containing Mixed-Layer Silicates from Szklary, Lower Silesia, Poland. Bull. BRGM sec. II, 3, 247–261.

Figures and tables:

Fig. 1. Orthophotograph showing the mining zones of the Falcondo deposit, including the location of the Loma Caribe peridotite belt in the Dominican Republic (left) and geological map of the same area (right) (modified from Haldemann *et al*., 1979).

Fig. 2. Schematic lateritic profile of the Falcondo deposit, showing the position of garnierites, and including major textural features, main mineral assemblage and Ni content of each zone of the profile. (modified from Lithgow *et al*., 1979; Lewis *et al*., 2006; Tauler *et al*., 2009). Total height of the profile is up to 60 m (Haldemann *et al*. 1979). Mineral abbreviations based on Whitney and Evans (2010). Legend: Hem = hematite, Gt = goethite, Srp = serpentine, Ol = olivine, En = enstatite, Cpx = clinopyroxene.

Fig. 3. Occurrence of garnierite mineralisations in the Falcondo deposit: a-b) garnierite outcrops in zone D; c) veinlets of type I crossing saprolite (zone D); d) garnierite veins cutting unweathered serpentinised peridotites (zone E+F); e) veinlets within upper saprolite horizon (zone C); f) veins; g) types II and IV in veins; h) vein of sepiolite-falcondoite; i) type III forming coatings in fractures; j) veins and coatings on joints with random orientations, k) garnierite mineralisation along a fault plane; l) slickenside with visible direction of movement; m) breccia of saprolite clasts cemented by sepiolite and quartz/silica; n) detail of sample collected from m). Legend: I-IV = types I-IV, Sep = sepiolite, Fal = falcondoite, Qz = quartz.

Fig. 4. Hand specimens of the samples selected for this paper: a) LC-100Aa. b) LC-100B, c) GAR-1, d) GAR-2, e) GAR-6, f) GAR-5, g) F-0, h) F-3. Legend: I-IV = types I-IV, sapr = saprolite fragment, Qz = quartz, Ni-Sep = Ni-sepiolite, Fal = falcondoite. See text for explanation.

Fig. 5. X-ray powder difractograms of garnierite types I to IV from the Falcondo Ni-laterite deposit studied in this paper. Black circles and triangles indicate the d-spacings of serpentine-like and talc-like structures, respectively. The lower segments correspond to quartz peaks from the standard coded 00-046-1045.

Fig. 6. Optical photomicrographs showing characteristic textures of the described garnierite typologies. a-b) Plane polarised light (a) and crossed polars image (b) of saprolite and type I garnierite. b) includes a backscattered electron image of the selected

area in the red box). c-d) Plane polarised light (c) and crossed polars image (d) of type II garnierite with brownish gray talc-like matrix (Tlc), saprolite and type IV garnierite. e) Plane polarised light image of type III garnierite envelopping euhedral quartz crystals, over a saprolite fragment. f) Crossed polars image of type IV botryoidal aggregates interstratified with quartz layers. g) Plane polarised light image of saprolite fragment wrapped by type IV in a matrix of rounded quartz and garnierite. h) Crossed polars image of type IV botryoidal aggregates in a matrix of rounded quartz and garnierite, crosscut by microcrystalline quartz veinlets. Legend: I-IV = types I-IV, sapr = saprolite fragment, Qz = quartz.

Fig. 7. a) Textural and compositional features of saprolite Ni-serpentine and quartz, b) photomicrograph of the selected area, and c) triangular diagram showing the spot analyses and the quantified pixels of the scanned area expressed as absolute frequency (color scale) from sample GAR-3b (200 nA). In the XR maps the scaled (color code) distribution of elements and elemental ratio is expressed in cations per fixed number of oxygens (i.e., charges) in the respective formula units. The mineral formulae were calculated using an internal standard of Ni-serpentine analysed in the scanned area. In the triangular diagram the total number of pixels plotted is 238721. All pixels were quantified using a spot analysis of serpentine as internal standard. Stoichiometric Mg and Ni end members of the solid solutions of interest are indicated for reference. Legend: Qz = quartz, Srp = serpentine, Srp* = oceanic hydrothermal serpentine, Ni-Srp = Ni-bearing serpentine, FeOx = Fe oxyhydroxides, Sep = sepiolite, Fal = falcondoite, Ker = kerolite, Pim = pimelite, Krp = karpinskite, Ni-Krp = Ni-karpinskite, Liz = lizardite, Nep = népouite.

Fig. 8. Textural and compositional features of a) Ni-bearing talc-like, b) quartz, and c) serpentine with the intermediate phase, d) photomicrograph of the selected area, and e) triangular diagram showing the spot analyses and the quantified pixels of the scanned area expressed as absolute frequency (color scale) from sample GAR-4a (200 nA). In the XR maps the scaled (color code) distribution of elements and elemental ratio is expressed in cations per fixed number of oxygens (i.e., charges) in the respective formula units. Mg, Fe and Ni are scaled uniformly in order to better compare mineral compositions. The mineral formulae were calculated using an internal standard of the same mineral analysed in the scanned area (talc-like or serpentine-like), except for the intermediate phase that was quantified using the same internal standard as serpentine-

like. The total number of pixels plotted in the triangular diagram is 262144. All pixels were quantified using a spot analysis of talc as internal standard. Stoichiometric Mg and Ni end members of the solid solutions of interest are indicated for reference. Legend: Qz = quartz, Srp = serpentine, Sep = sepiolite, Fal = falcondoite, Ker = kerolite, Pim = pimelite, Krp = karpinskite, Ni-Krp = Ni-karpinskite, Liz = lizardite, Nep = népouite.

Fig. 9. a) Textural and compositional features of Ni-bearing talc-like and quartz, b) photomicrograph of the selected area, and c) ternary diagram showing the spot analyses and the quantified pixels of the scanned area expressed as absolute frequency (color scale) from sample LC-100Bb (200 nA). In the XR maps the scaled (color code) distribution of elements and elemental ratio is expressed in cations per fixed number of oxygens (i.e., charges) in the respective formula units. Mg and Ni are scaled uniformly in order to better compare mineral compositions. The mineral formulae were calculated using an internal standard of the same mineral analysed in the scanned area. In the triangular diagram the total number of pixels plotted is 259030. All pixels were quantified using a spot analysis of talc as internal standard. Stoichiometric Mg and Ni end members of the solid solutions of interest are indicated for reference. Legend: Qz = quartz, Sep = sepiolite, Fal = falcondoite, Ker = kerolite, Pim = pimelite, Krp = karpinskite, Ni-Krp = Ni-karpinskite, Liz = lizardite, Nep = népouite.

Fig. 10. a-d) Textural and compositional features of Ni-sepiolite and quartz, e) photomicrograph of the selected area, and f) ternary plot showing the spot analyses and the quantified pixels of the scanned area expressed as absolute frequency (color scale) from sample FLC-2 (100 nA). Maps show the distribution of Mg (a), Ni (b), Si (c) in sepiolite and quartz, and Ni in quartz (d). In the XR maps the scaled (color code) distribution of elements is expressed in cations per fixed number of oxygens (i.e., charges) in the respective formula units. In the upper figures, Mg and Ni are scaled uniformly in order to better compare mineral compositions. The mineral formulae were calculated using an internal standard of sepiolite analysed in the scanned area. The Ni image for quartz is scaled to 0.1 cations/pfu in order to show the chemical zoning of this mineral. The image is set on a greyscale image of Ni to show the basic chemical/textural relations of the scanned area. The total number of pixels in the triangular diagram is 140431. All pixels were quantified using the same spot analysis of sepiolite. Stoichiomentric Mg and Ni end members of the sepiolite solid solution are indicated for

reference. Legend: Qz = quartz, Sep = sepiolite, Fal = falcondoite, Ker = kerolite, Pim = pimelite, Krp = karpinskite, Ni-Krp = Ni-karpinskite, Liz = lizardite, Nep = népouite.

Fig. 11. Ternary plots showing the compositions of the analysed garnierites compared to the data from other localities, plotted as calculated in atoms per formula unit. a) serpentine-like garnierites, b) talc-like garnierites, c) garnierites of the sepiolite-falcondoite series (including data from Tauler et al., 2009 and this study), d) garnierite compositions from the literature, according to the description of the author(s) in the corresponding paper. Literature data: Ross et al. (1928), Pecora et al. (1949), Kato (1961), Faust (1966), Naganna and Phene (1968), DeWaal (1970), Brindley and Hang (1973), Maksimović (1973), Springer (1974), Brindley and Wan (1975), Nickel and Bridge (1975), Springer (1976), Esson and Carlos (1978), Brindley *et al*. (1979), Poncelet *et al*. (1979), Gerard and Herbillon (1983), Manceau and Calas (1985), Ducloux et al. (1993), Song *et al*. (1995), Talovina *et al*. (2008), Wells *et al*. (2009). Stoichiomentric Mg and Ni end members of the sepiolite solid solution are indicated for reference. Legend: Sep = sepiolite, Fal = falcondoite, Ker = kerolite, Pim = pimelite, Krp = karpinskite, Ni-Krp = Ni-karpinskite, Liz = lizardite, Nep = népouite.

Table 1. Summary of the characteristics of the twelve samples selected for this paper, including description, mineralogy, average structural formula and range of Ni content.

Table 2. Representative EMP analysis (in weight percent) and structural formulae (in atoms per formula unit) of the studied garnierite typologies (I-IV), saprolite serpentine and Ni-sepiolite-falcondoite, ordered by mineral and Ni content. Notes: na = not analysed, (*) = calculations according to the formulae given by Brindley and Hang (1973).

TABLE 1

SAMPLES	DESCRIPTION	TYPE(S)	XRD	STRUCTURAL FORMULA	NiO CONTENT (%.wt)
LC-100A, LC-101	Saprolite breccia cemented by type I (yellowish pale green), in turn wrapped by type IV (bluish green) (Fig. 4a).	type I (yellowish pale green) and IV (bluish green)	7 Å (Fig. 5a)	$Mg_{1.73}Ni_{1.37}Fe_{0.03}Si_{3.92}O_{10}(OH)_2$ (type I)	0.84–14.12
LC-100B	Saprolite breccia cemented by type II (apple green), in turn wrapped by type IV (bluish green) (Fig. 4b).	type II apple green) and IV (bluish green)	7 Å and minor talc-like impurities 10 Å (Fig. 5b)	$Mg_{1.58}Ni_{0.92}Al_{0.05}Fe_{0.03}Si_{2.17}O_5(OH)_4$ (type II)	11.85–26.62
GAR-1	Massive dark green aggregate (Fig. 4c), breccia (Fig. 4d).	type III (dark green)	7 + 10 Å (Fig. 5c)	$Ni_{1.79}Mg_{0.57}Si_{2.31}O_5(OH)_4 \cdot n(H_2O)$ (type III)	29.08–49.71
GAR-2, GAR-3	Saprolite breccia cemented by type III (dark green) (Fig. 4e).	type III (dark green)			
GAR-6	Saprolite breccia cemented by type IV (bluish green) (Fig. 4f).	type IV (bluish green)	10 Å (Fig. 5d)	$Mg_{1.56}Ni_{1.53}Si_{3.94}O_{10}(OH)_2 \cdot (H_2O)$ (type IV)	7.77–44.39
GAR-4	Aggregates of type IV (bluish green) in a matrix of a second generation of garnierite and microcrystalline quartz (Fig. 4g).	type IV (bluish green)			
FLC-4, FLC-2, GAR-7	White to greenish white sets of wavy sheets of Ni-sepiolite (Fig. 4h).	type V (sepiolite-falcondoite)	12 Å	$Mg_{5.76}Ni_{1.69}Si_{12.22}O_{15}(OH)_2 \cdot 6(H_2O)$ (type V)	1.15–27.89

FLC-3	Pale green sets of wavy sheets of Ni-sepiolite-falcondoite (Fig. 4h).	type V (sepiolite-falcondoite)	12 Å		

TABLE 2

ID #	A-i-14	LC100 A1g221	A-b-46	A-b-41	lc100 1-62	lc100 1-28	lc100 1-61	GAR 3-pto1-7	gar3b-81	GAR1-a2	LC10 1bc13	LC10 1b-c7	LC100 Abc13	GAR 7-a7	FAL3pto1_11
Mineral	Srp	Srp	Srp	Srp	Srp	Srp	Srp	Srp	Srp	Srp	Tlc	Tlc	Tlc	Sep	Sep
Sample	LC-101	LC-100A	LC-101	LC-101	LC-100B	LC-100B	LC-100B	GAR-3b	GAR-3b	GAR-1b	LC-101	LC-101	LC-100A	GAR-7	FLC-3
Type	saprolite	saprolite	type I	type I	type II	type II	type II	type III	type III	type III	type IV	type IV	type IV	sep-falc	sep-falc
SiO2	40.15	43.58	40.76	40.72	40.86	42.57	41.79	44.27	41.42	37.89	52.69	52.94	48.86	60.64	49.56
TiO2	0.03	0.00	0.03	0.00	0.02	0.03	0.00	0	0.02	0	0.00	0.00	0.00	0.01	0.00
Al2O3	0.17	0.65	0.02	0.02	2.46	1.26	0.22	0.01	0.05	0	0.00	0.01	0.09	0.00	0.31
Cr2O3	0.49	0.01	0.03	0.12	0.03	0.00	0.03	0.01	0.01	0.01	0.00	0.00	0.01	0.00	0.00
Fe2O3	5.76	1.70	5.15	8.91	0.77	0.50	0.36	0.04	0.03	0.02	0.02	0.02	0.01	0.10	0.09
MnO	0.02	0.01	0.00	0.01	0.04	0.00	0.03	0.03	0.01	0	0.00	0.00	0.02	0.00	0.02
MgO	36.46	35.88	36.40	33.36	28.97	21.62	12.62	10.87	7.86	5.25	18.63	13.08	4.55	22.62	10.79
NiO	2.91	6.42	2.90	5.33	11.85	21.54	29.14	32.42	40.67	46.06	16.09	25.22	40.70	7.73	23.36
CaO	0.02	0.00	0.00	0.07	0.05	0.03	0.02	0	0.02	0	0.04	0.09	0.02	0.05	0.00
Sum Ox%	86.05	88.26	85.32	88.61	85.05	87.55	84.25	87.69	90.11	89.24	87.53	91.61	94.30	91.17	84.27
Si	1.945	2.049	1.981	1.955	2.046	2.166	2.308	2.366	3.719	2.274	3.574	2.197	3.453	3.964	3.988	3.909	12.022	11.768
Al	0.010	0.000	0.001	0.001	0.000	0.000	0.014	0.001	0.001	0.003	0.005	0.000	0.000	0.000	0.001	0.008	0.000	0.087
Fe3+	0.045	0.000	0.018	0.044	0.000	0.000	0.000	0.000	0.003	0.000	0.002	0.000	0.002	0.001	0.001	0.001	0.000	0.016
sum [IV] (T)	**2.000**	**2.049**	**2.000**	**2.000**	**2.046**	**2.166**	**2.322**	**2.367**	**3.722**	**2.277**	**3.581**	**2.197**	**3.455**	**3.965**	**3.990**	**3.918**	**12.022**	**11.871**
Ti	0.001	0.000	0.001	0.000	0.001	0.001	0.000	0.000	0.000	0.001	0.001	0.000	0.000	0.000	0.000	0.000	0.001	0.000
Al	0.000	0.036	0.001	0.001	0.145	0.076	0.014	0.001	0.000	0.003	0.000	0.000	0.000	0.000	0.001	0.008	0.000	0.087
Cr	0.019	0.000	0.001	0.005	0.001	0.000	0.001	0.000	0.001	0.000	0.001	0.000	0.001	0.000	0.000	0.001	0.000	0.000
Fe3+	0.165	0.060	0.170	0.278	0.029	0.019	0.015	0.002	0.000	0.001	0.000	0.001	0.000	0.000	0.000	0.000	0.015	0.000
Mn	0.001	0.000	0.000	0.000	0.002	0.000	0.001	0.001	0.002	0.000	0.001	0.000	0.000	0.000	0.000	0.001	0.000	0.004
Mg	2.633	2.514	2.637	2.387	2.162	1.640	1.039	0.866	1.361	0.643	1.011	0.454	0.713	2.089	1.469	0.543	6.685	3.819
Ni	0.113	0.243	0.113	0.206	0.477	0.882	1.295	1.394	2.191	1.796	2.823	2.149	3.377	0.974	1.528	2.619	1.233	4.462
Ca	0.001	0.000	0.000	0.004	0.003	0.002	0.001	0.000	0.000	0.001	0.002	0.000	0.000	0.003	0.007	0.002	0.011	0.000
sum [VI] (O)	**2.935**	**2.818**	**2.751**	**2.595**	**2.670**	**2.541**	**2.352**	**2.263**	**3.559**	**2.442**	**3.840**	**2.604**	**4.092**	**3.064**	**2.999**	**3.165**	**7.933**	**8.301**
T / O	0.668	0.740	0.790	0.880	0.821	0.883	0.988	1.046	0.933	0.844	1.294	1.330	1.238	1.516	1.428
Tlc fraction (*)	0.001	0.110	0.184	0.319	0.232	0.324	0.482	0.569	0.400	0.266	0.940	0.996	0.857	-	-
Srp fraction (*)	0.999	0.890	0.816	0.681	0.768	0.676	0.518	0.431	0.600	0.734	0.060	0.004	0.143	-	-
Ni/Mg	0.043	0.097	0.043	0.086	0.221	0.538	1.246	1.609	2.792	4.734	0.466	1.040	4.827	0.184	1.168
oxygens	7	7	7	7	7	7	7	7 11	7 11	7 11	11	11	11	32	32

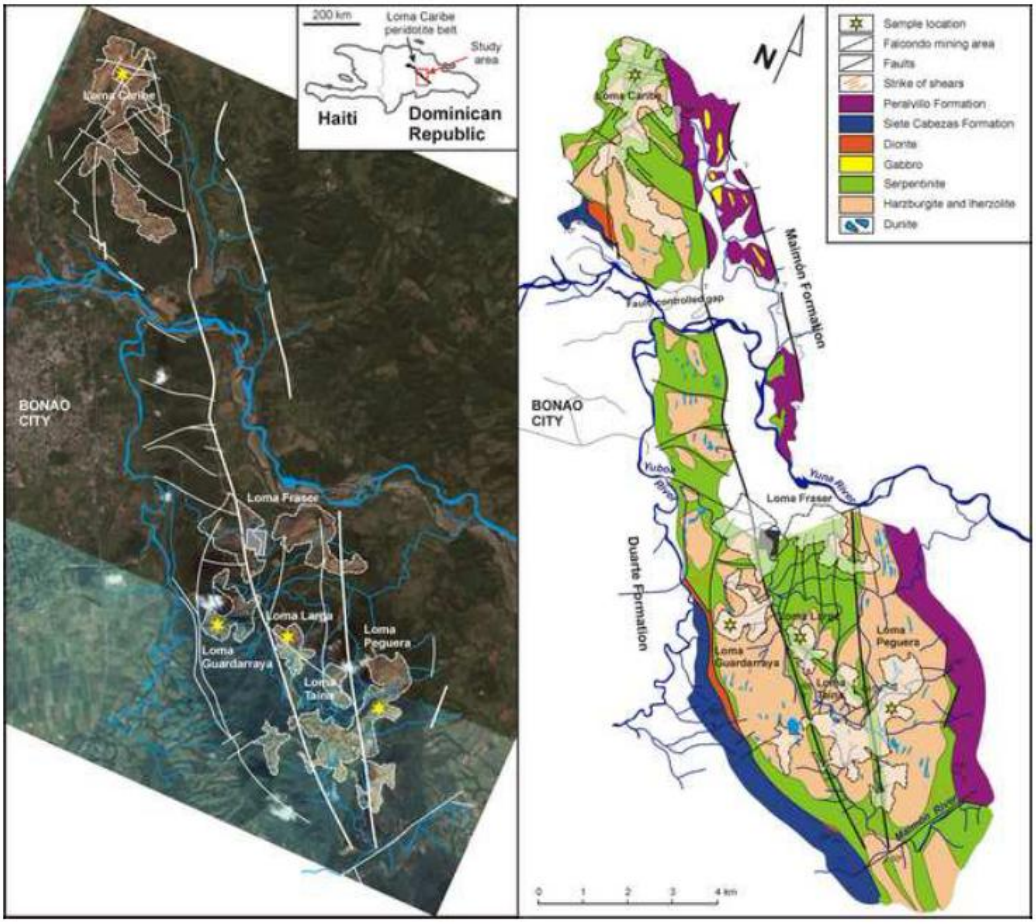

Figure 1

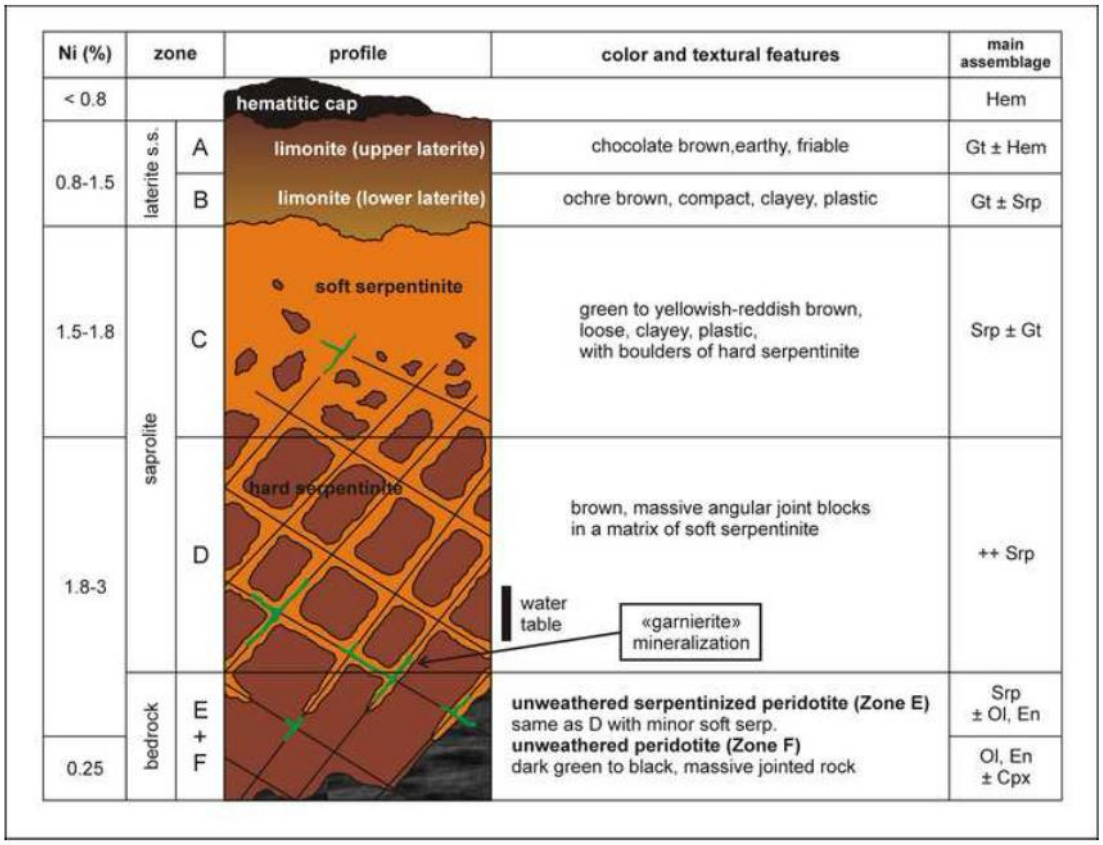

Figure 2

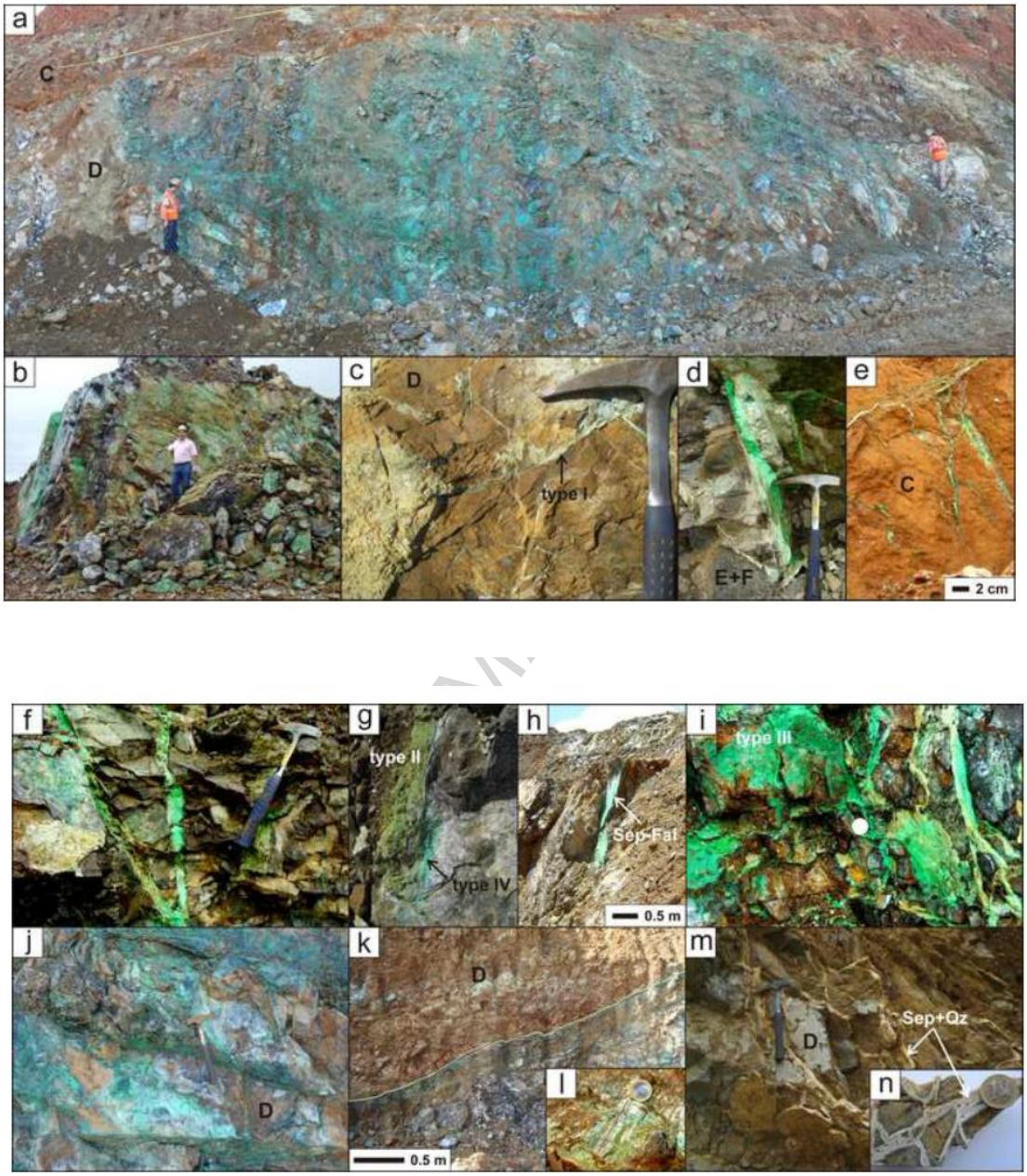

Figure 3

Figure 4

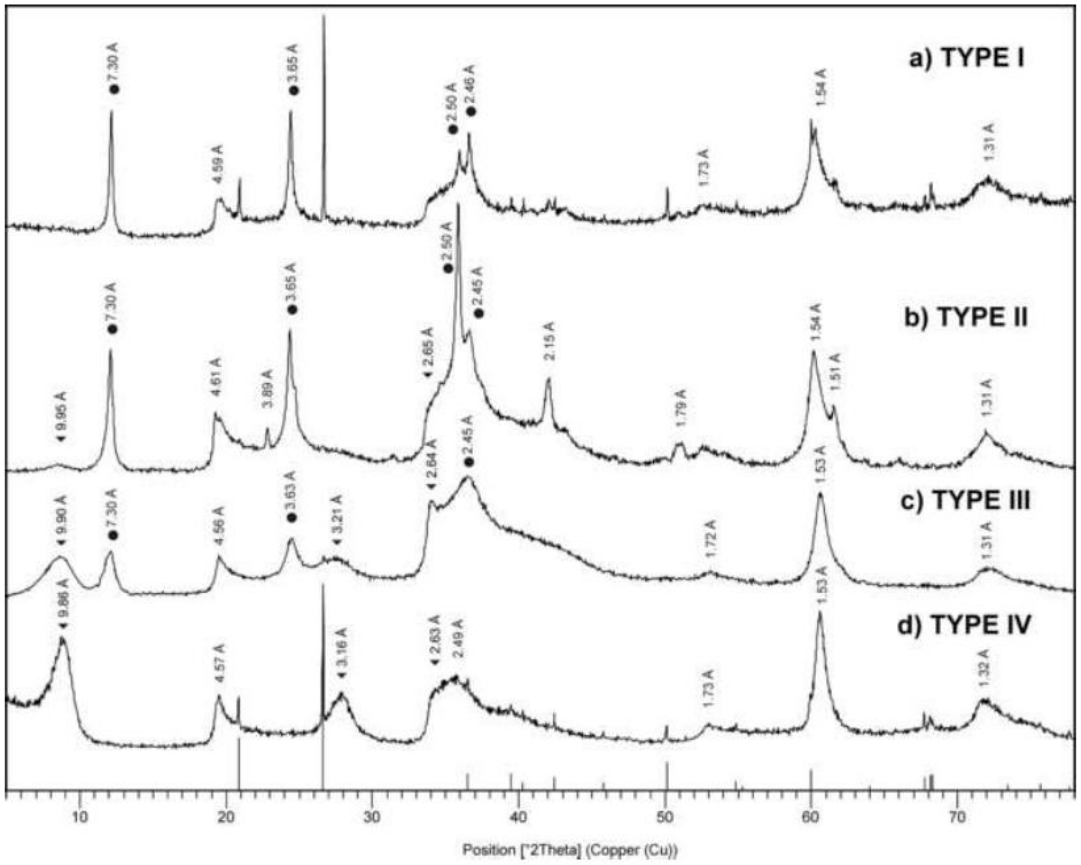

Figure 5

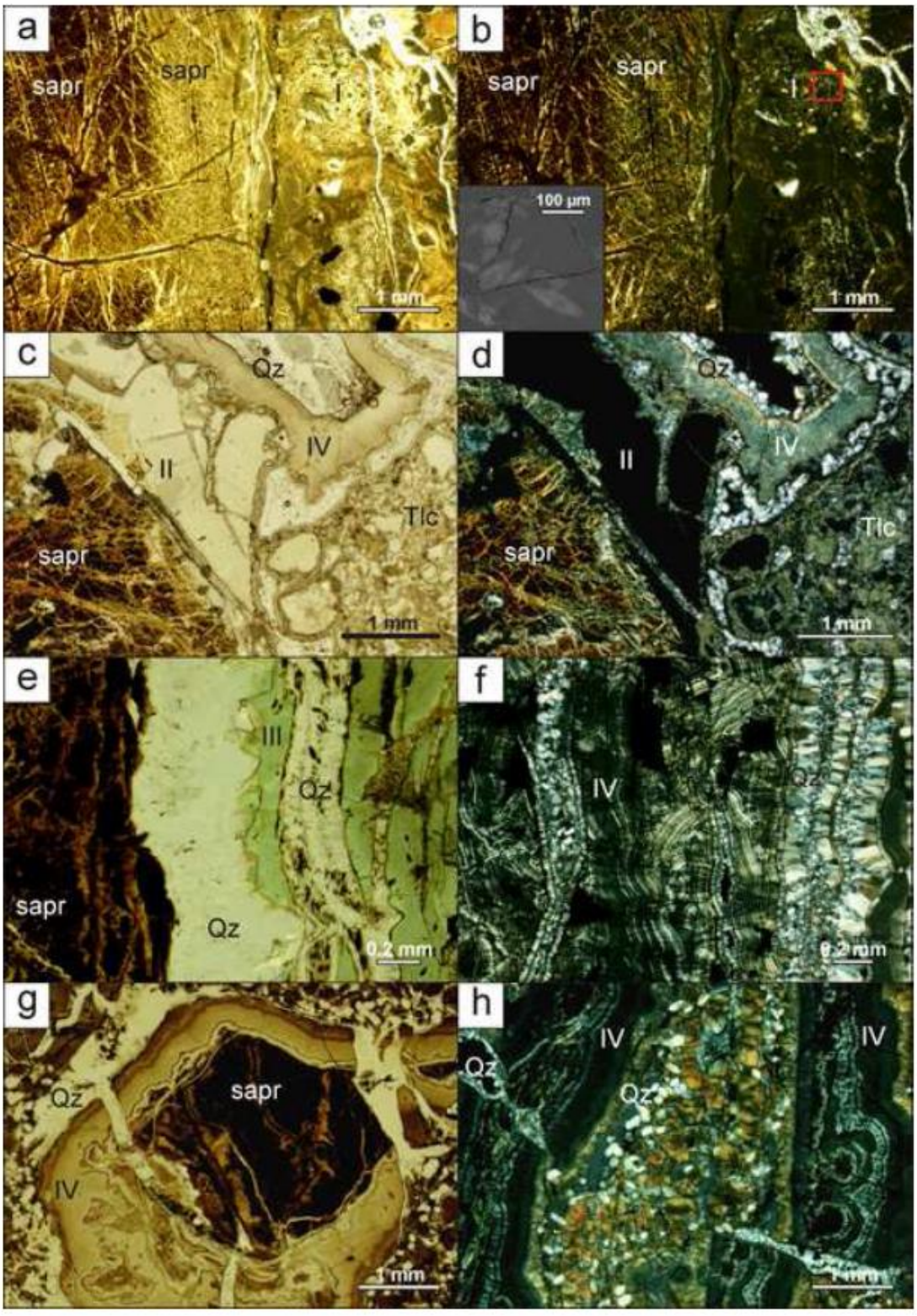

Figure 6

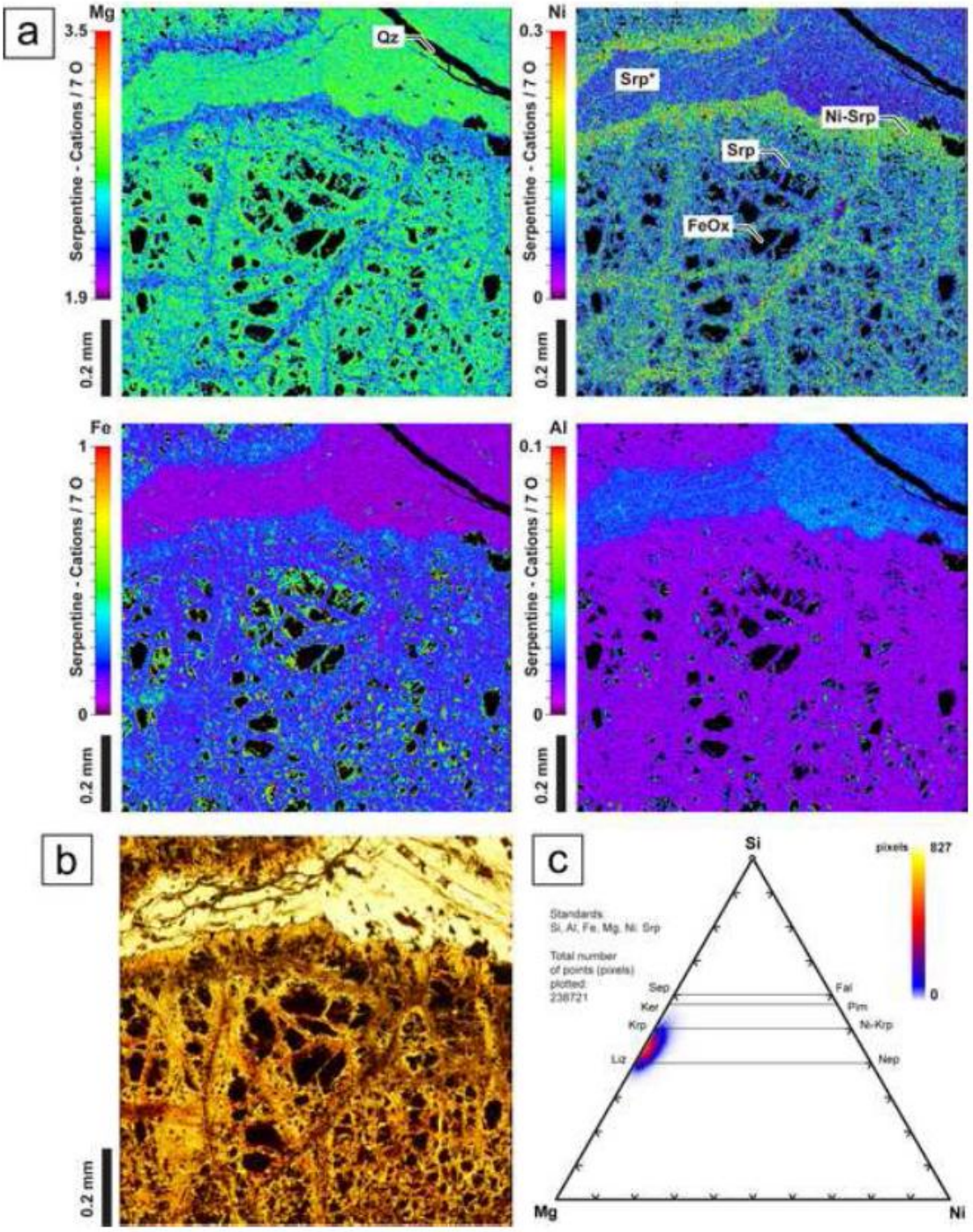

Figure 7

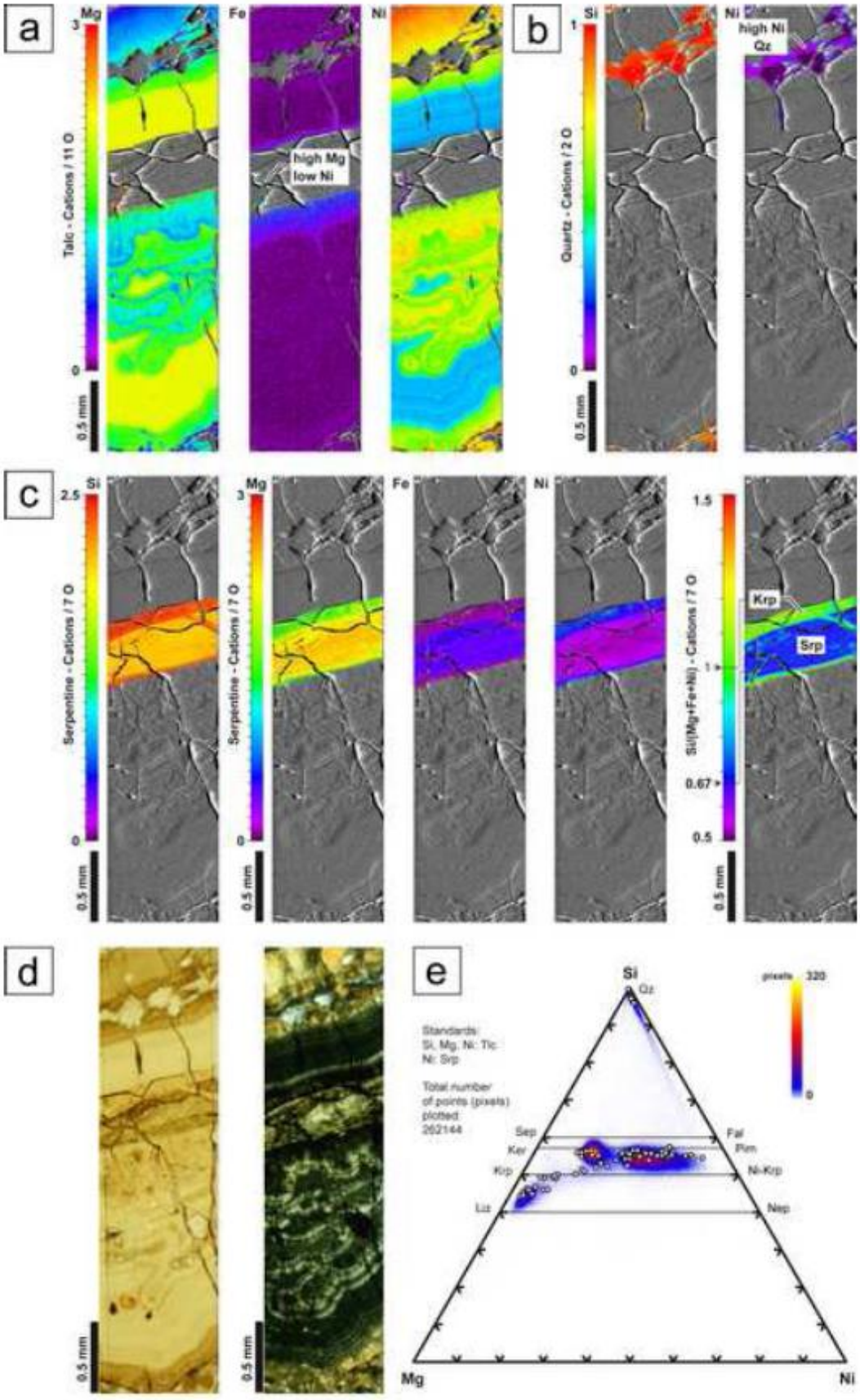

Figure 8

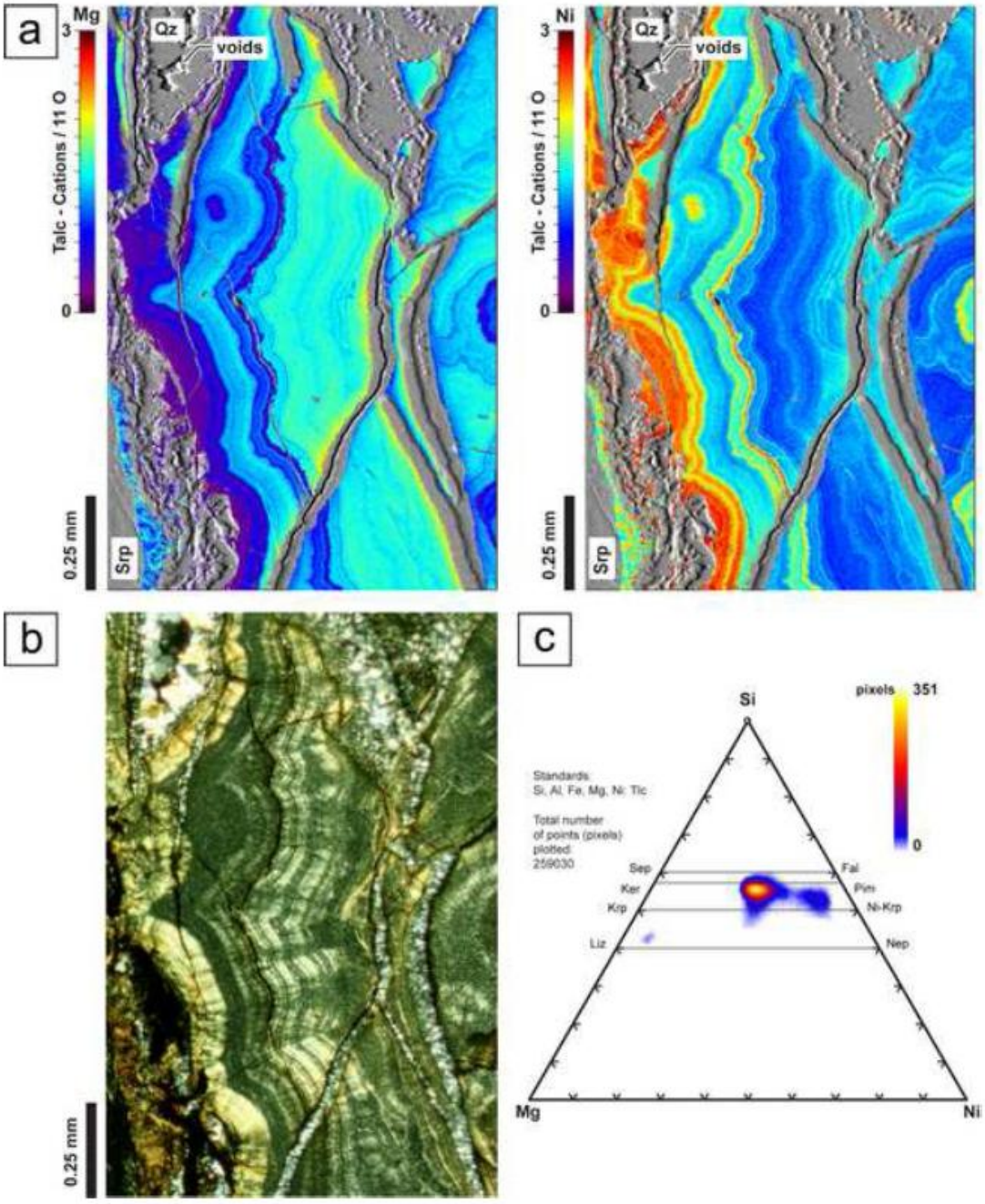
a
Mg
3
Talc - Cations / 11 O
0
Qz
voids
0.25 mm
Srp
Ni
3
Talc - Cations / 11 O
0
Qz
voids
0.25 mm
Srp
b
0.25 mm
c
Si
pixels 351
0
Standards:
Si, Al, Fe, Mg, Ni: Tlc
Total number
of points (pixels)
plotted:
259030
Sep
Ker
Krp
Liz
Fal
Prn
Ni-Krp
Nep
Mg
Ni

Figure 9

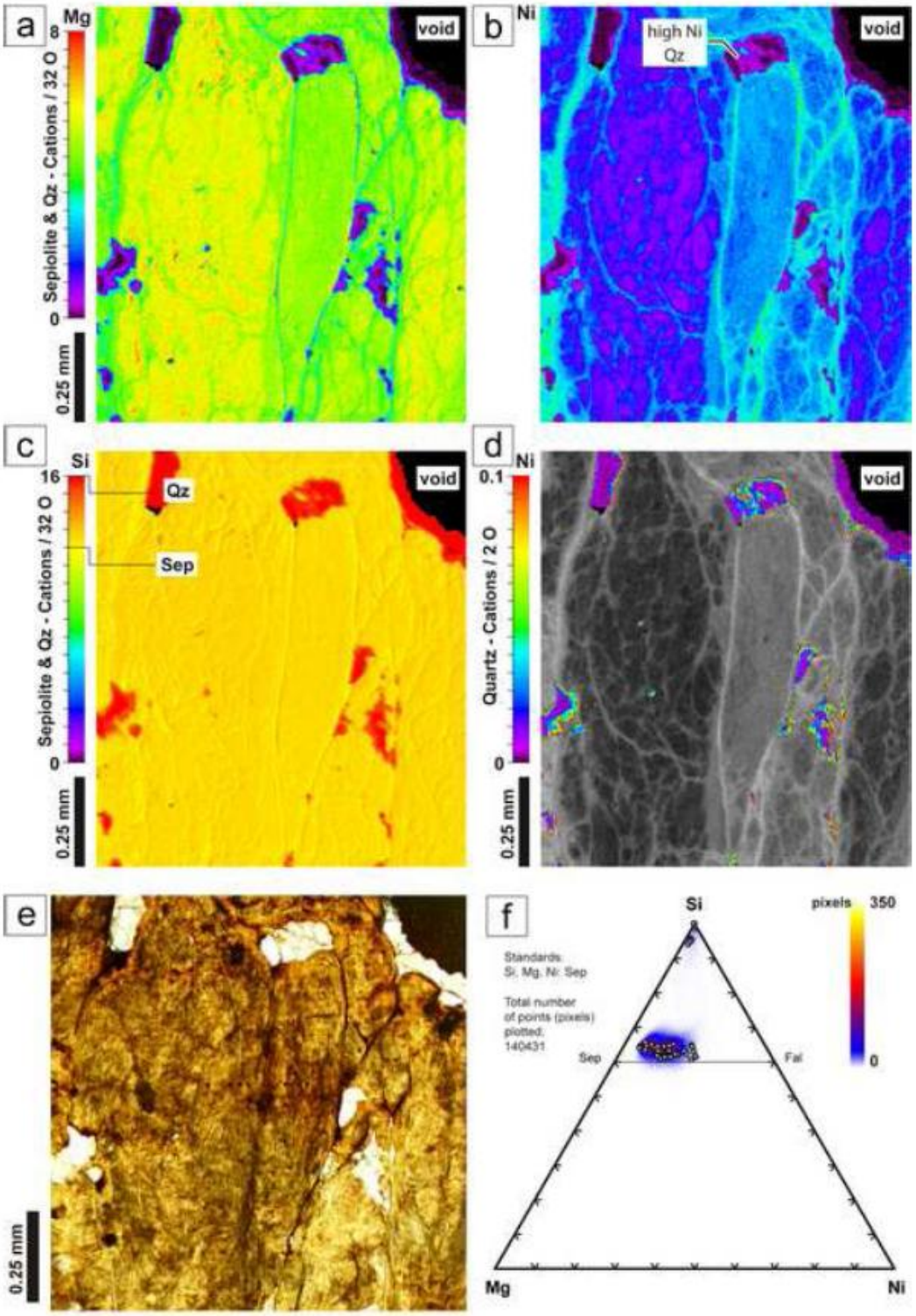

Figure 10

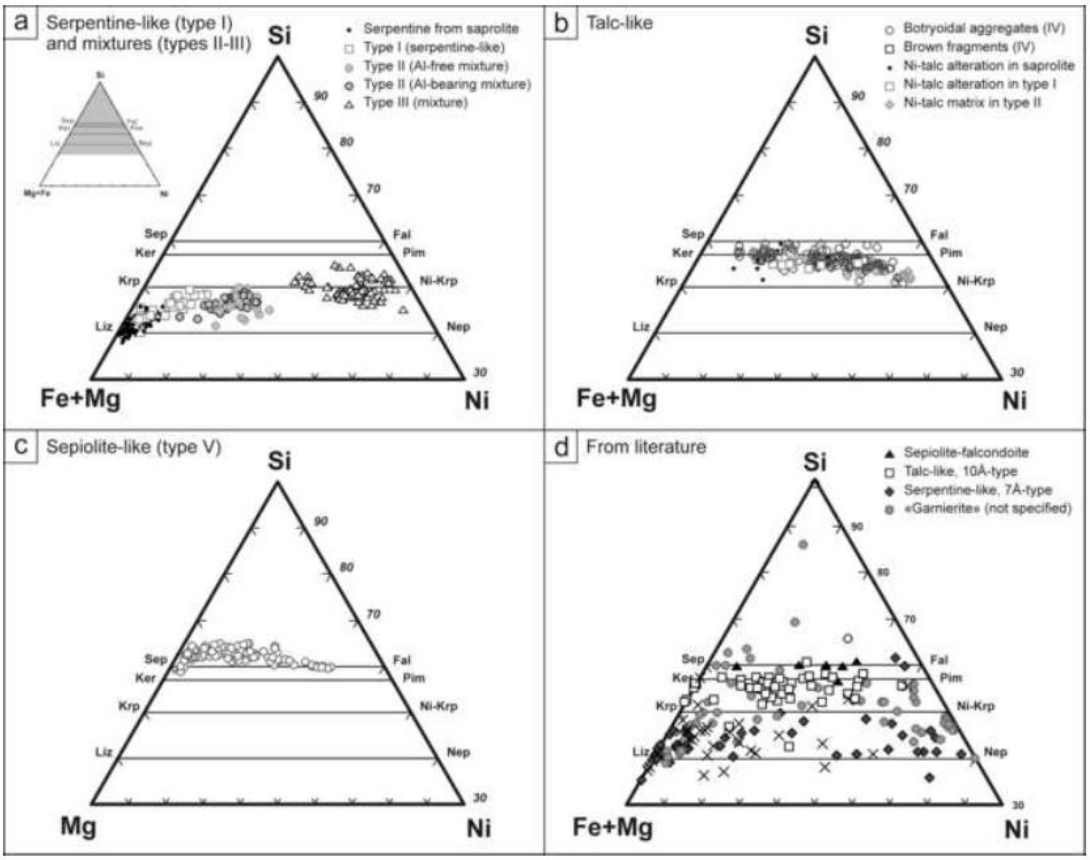

Figure 11

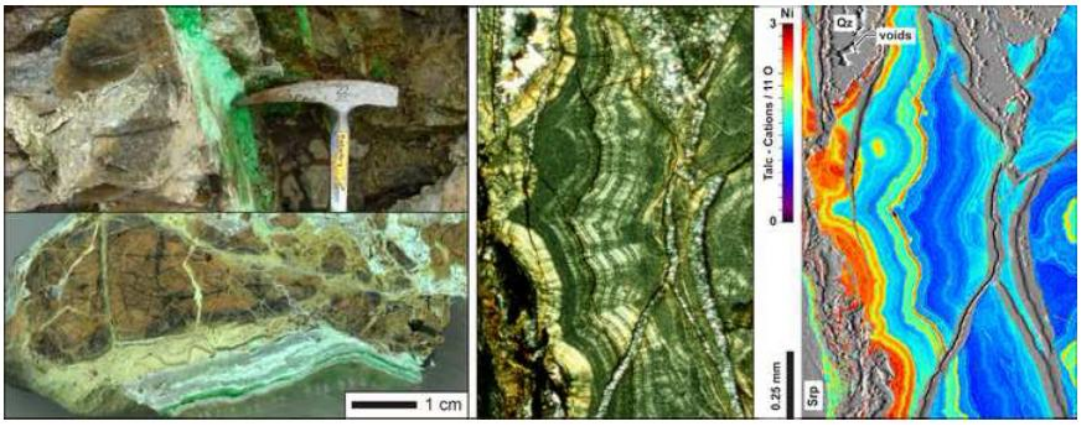

Graphical abstract

Highlights

- Garnierites from Falcondo precipitated in a tectonically active regime.

- Five types were identified: serpentine-, talc-, sepiolite-like and mixtures.

- Garnierite precipitation occurred in successive stages progressively.

- The main garnierite in Falcondo is talc-like, and shows one of the highest Ni contents.

- The variation of garnierite mineralogy has implications on ore processing.